TECHNICAL REPORT 2050
September 2014

Making the Effects of Varying the Capacitance, Resistance, Temperature, and Frequency Dependence for HTS Josephson Junctions, DC SQUIDS, and DC bi-SQUIDs

Susan Berggren
Benjamin Taylor
Anna Leese De Escobar

SSC Pacific
San Diego, CA 92152-5001

TECHNICAL REPORT 2050
September 2014

Making the Effects of Varying the Capacitance, Resistance, Temperature, and Frequency Dependence for HTS Josephson Junctions, DC SQUIDS, and DC bi-SQUIDs

Susan Berggren
Benjamin Taylor
Anna Leese De Escobar

SSC Pacific
San Diego, CA 92152-5001

SSC Pacific
San Diego, California 92152-5001

K. J. Rothenhaus, CAPT, USN
Commanding Officer

C. A. Keeney
Executive Director

ADMINISTRATIVE INFORMATION

The work described in this report was performed by the Applied Research Branch (Code 71730) of the Advanced Systems and Applied Sciences Division (Code 71700), Space and Naval Warfare Systems Center Pacific (SSC Pacific), San Diego, CA. The Naval Innovative Science and Engineering (NISE) Program at SSC Pacific funded this Applied Research project.

.

Released by
K. Simonsen, Head
Applied Research Branch

Under authority of
A. D. Ramirez. Head
Advanced Systems and
Applied Sciences Division

EXECUTIVE SUMMARY

OBJECTIVE

The objective of this research was to explore the effects of altering the third junction in an array of bi-superconducting quantum interference devices (bi-SQUIDs) on the overall performance characteristics. The third junction could be altered by either fabricating it using a different method, such as ion beam milling or ion damage, or with junctions specifically designed to exploit certain properties, as with multiferroic junctions. First, an exploration was performed to review the effects of capacitance and noise terms for a single junction, and a single SQUID. This was done to validate the simulations and to create a baseline with which to compare the new work. Once the effects were characterized, a single bi-SQUID and array of bi-SQUIDs were examined that had noise temperature and capacitance terms on the bisecting junctions only. This setup represents a device with traditional main junctions and different third junction, which could be used to precisely design the array for tuneabilty or filter-like effects by controlling the linearity and voltage swing of the anti-peak. The linearity and voltage swing are important for increased gain and improved accuracy. Finally, a frequency dependence was added to the third junction to determine the effects of having a multiferroic third junction.

RESULTS

We determined that for a single junction and single SQUID, capacitance is detrimental, as it causes hysteresis. Even a small amount of hysteresis in the I-V curve destroyed the voltage swing in the $V(x_e)$ curve, which is the response we are trying to manipulate for signal detection. A decrease in the junction resistance counteracts the hysteresis arising from the capacitance. A large resistance negatively impacts junction performance and has an even stronger impact on hysteresis since $\beta_c \propto R^2$ while $\beta_c \propto C$. A small amount of temperature noise also decreases any hysteresis present; however, it also decreases the junction critical current. When hysteresis is present in the I-V curve, the bias current can be decreased to increase the voltage swing; however, this results in hysteresis in the $V(x_e)$ curve.

When we just include the capacitance and temperature terms on the bisecting Josephson junction, and leave the outer loop main junctions as ideal junctions, their impact on the $V(x_e)$ curve are decreased. The temperature term counteracted the effects of a large third-junction critical current on the $V(x_e)$ curve when there were small capacitance and resistance values. Gain is increased as we couple the SQUID or bi-SQUID devices together into arrays, so when we fabricate the prototype bi-SQUID sensor, we anticipate having tens of thousands of bi-SQUIDs in the array. As with the single bi-SQUID, the impact of the capacitance and temperature terms on the $V(x_e)$ curve was decreased. From this we can surmise that if care is taken with the main two Josephson junctions, then the bisecting junction can be fabricated with an inferior method and still result in a good device. An inferior method could be used to overcome design layout issues or for the properties gained by using them (i.e., multiferroics).

For the frequency dependence, we determined that we can control the signal detection if there is a frequency dependence on the critical current of the third junction. For a very basic example, if we could find a method that results in a large i_{c3} value (≈ 10) for large frequencies, and have a value close to $i_{c3} = 1.0$ in a range where the signal strength is small, and $i_{c3} = 0$ elsewhere, we could have a device that acts like a low-pass filter and amplifies the signals further in the determined range. The value of the third-junction critical current had a much larger effect on the frequency dependence than the changes to the time constant.

RECOMMENDATIONS

Based on the results of this study, we determined that a modification to the third junction is a viable approach to introduce a desired frequency dependence and/or control of the linearity and voltage swing of the anti-peak. This study, while extensive, was by no means exhaustive, and a significant amount of work remains to fully examine the different effects.

CONTENTS

Figures

1. INTRODUCTION

Superconductive materials have the unique property that they lose all resistance to electric current when cooled below a critical temperature. A Josephson junction is a thin layer of insulating material separating two superconductors that is thin enough for electrons to tunnel through. Two Josephson junctions placed in parallel into a ring of superconducting material form what is known as a DC Superconducting Quantum Interference Device (SQUID). SQUIDs can sense minute magnetic fields approaching 10^{-15} Tesla. These SQUIDs can be arranged in arrays with different coupling schemes and parameter values to create a combined voltage flux response ($V(x_e)$). Control over the linearity of $V(x_e)$ is important for increased gain and improved accuracy.

Increasing the number of SQUIDs, N, in an array increases the detected signal amplitude as a function of N, while the noise is increased as a function of $N^{1/2}$ [1]. A single SQUID has two Josephson junctions in a ring of superconducting material. A third junction bisecting the superconducting loop is added to increase the linearity of the voltage response output [2]. This device is called a bi-SQUID. We will explore using the effects of using a different material and/or method on the bisecting Josephson junction for high temperature superconductor (HTS) $YBa_2Cu_3O_{7-\delta}$ (YBCO) bi-SQUIDs.

This technical report is organized as follows. First, we review the effects of capacitance and noise terms for a single junction [3–6]. We then expand the analysis to a single SQUID [7]. Next, we compare the single SQUID with a single bi-SQUID that has noise temperature and capacitance terms on the bisecting junction only. Then we explore the effects of noise temperature and capacitance on an array of 50 bi-SQUIDs. Finally, we look at effects of frequency dependence of the third junction. The effects explored are those that could arise from junctions either fabricated using a different method, such as ion beam milling or ion damage [8–11], or with junctions specifically designed to exploit certain properties as with multiferroic junctions [12–14]. Precisely designing the junctions could result in benefits such as tuneabilty or filter-like effects.

2. SINGLE JUNCTION AND HYSTERESIS

First, we examine the single Josephson junction dynamics and the effect of capacitance, resistance, and temperature.

2.1 MODELING EQUATIONS

In Figure 1 we show the schematic diagram of a single Josephson junction. We model a single resistively and capacitively shunted Josephson junction, where the X represents a Josephson junction, I_1 is the current through the junction, and I_B is the DC bias current.

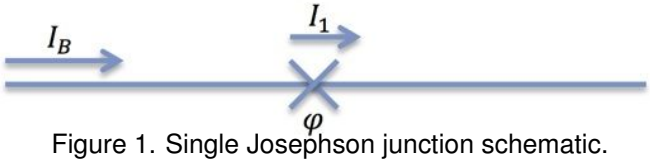

Figure 1. Single Josephson junction schematic.

The equation to model the voltage-current response, which includes a temperature noise term, is

$$\frac{\hbar C}{2eI_0}\ddot{\varphi} + \frac{\hbar}{2eRI_0}\dot{\varphi} = \frac{I_1}{I_0} - \frac{I_C}{I_0}\sin\varphi + \frac{\kappa_B T}{I_0^2 R}2\delta(t-t'),$$

where $\hbar$ is Plank's constant, C is the junction capacitance, e is the charge of an electron, I_0 is the junction critical current, R is the junction resistance, κ_B is Boltzmann's constant, T is the temperature in Kelvin, I_C is the junction critical current accounting for fabrication imperfections, φ is the phase difference across the junction, and $\delta(t-t')$ is a Gaussian noise delta function. Other terms we are disregarding for the moment are the second harmonic ($q\sin 2\varphi$) and the AC drive current ($I_d \sin\omega_d t$) [6]. The AC drive current results in a phenomenon known as Shappiro steps [15]. For our application, we only apply a DC drive current. Setting $\tau = \omega_0 t = \dfrac{2eRI_0}{\hbar}t$ (the Josephson time constant) gives the dimensionless ordinary differential equation (ODE):

$$\beta_C\frac{d^2\varphi}{d\tau^2} + \frac{d\varphi}{d\tau} = i_1 - i_c\sin\varphi + \frac{2e\kappa_B T}{I_0\hbar}2\delta(\tau-\tau'),$$

where $\beta_c = \dfrac{2eCR^2I_0}{\hbar}$ is called the McCumber parameter and is found by

$$\frac{\hbar C}{2eI_0}\omega_0^2 = \frac{\hbar C}{2eI_0}\left(\frac{2eRI_0}{\hbar}\right)^2 = \frac{2eCR^2I_0}{\hbar}.$$

From the drawing and Kirchhoff's current law, we have that $i_1 = i_B$, so the second order differential equation we need to solve to get the current voltage (I-V) curve is

$$\beta_C\frac{d^2\varphi}{d\tau^2} + \frac{d\varphi}{d\tau} = i_B - i_c\sin\varphi + \frac{2e\kappa_B T}{I_0\hbar}2\delta(\tau-\tau'),$$

where

$$V = \frac{\hbar}{2e}\dot{\varphi} = RI_0\frac{d\varphi}{d\tau} = V_0\frac{d\varphi}{d\tau}.$$

Splitting the second order differential equation into two dependent first-order differential equations yields

$$\begin{aligned}\frac{d\varphi}{d\tau} &= v \\ \beta_C\frac{dv}{d\tau} &= i_B - i_c\sin\varphi + \frac{2e\kappa_B T}{I_0\hbar}2\delta(\tau-\tau') - v. \end{aligned} \quad (1)$$

Equation (1) is integrated in Matlab using the Euler–Maruyama algorithm with a time span of $\tau = (0, 2^{20})\Delta\tau$ over a range of i_B values from negative to positive and then sweeping back positive to negative. This time-dependent voltage response output is then filtered through a moving average filter and plotted against i_B.

2.2 PARAMETERS

The parameters related to the modeling of Equation (1) are summarized below:

$$\begin{aligned} h &= 2\pi\hbar = 6.6260696 \times 10^{-34}\text{Js} \\ \Phi_0 &= \frac{h}{2e} = 2.067834 \times 10^{-15}\text{Wb} \\ V_0 &= RI_0 \\ \tau &= \frac{2eRI_0}{\hbar}t = \frac{2\pi RI_0}{\Phi_0}t = 2\pi V_0\Phi_0 t \\ \beta_C &= \frac{2eCR^2I_0}{\hbar} = \frac{2\pi CR^2I_0}{\Phi_0} = \frac{2\pi(RC)(I_0R)}{\Phi_0} \\ K_P &= \frac{T}{I_0} \times 10^{-7} \end{aligned}$$

2.3 SINGLE JUNCTION SIMULATION RESULTS

A small amount of temperature noise (also known as thermal noise) and capacitance with a normalized amount of resistance, in a single junction produces the behaviors as shown in Figure 2. Here, $K_P = 0.01$, $R = 1.0$, and $C = 0.1$. The plot on the left is the voltage over time of the junction as the bias current i_B is varied from -4.0 to 4.0 and back to -4.0. The plot on the right is the voltage plotted against i_B using a moving average filter. There are no observable effects of noise, and no hysteresis. This is an example of an ideal junction's dynamics.

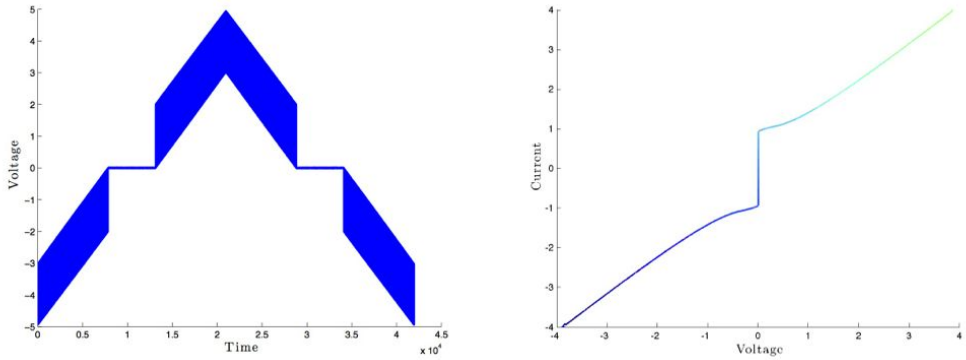

Figure 2. $V(t)$ curve (left) and I-V curve (right) with $K_P = 0.01$, $R = 1.0$, and $C = 0.1$.

Increasing the capacitance C increases the amount of hysteresis present in the I-V curve. For $K_P = 0.01$, $R = 1.0$, and $C = 2.0$ (see Figure 3). The amplitude is decreased in the time series plot of the voltage on the left. The hysteresis in the I-V curve on the right allows you to see the time progression color change. At time zero, the line is red then goes to orange, yellow, green, and ends at blue. The hysteresis occurs when the current increases from negative to positive and delays when the response enters the superconductive state. A current with magnitude smaller than the critical current is needed. Once there, the junction stays in at zero voltage until the positive critical current is reached. On the path from positive to

negative, the same thing happens but this time the delay is on the positive side and the junction stays at zero voltage until the negative critical current is reached.

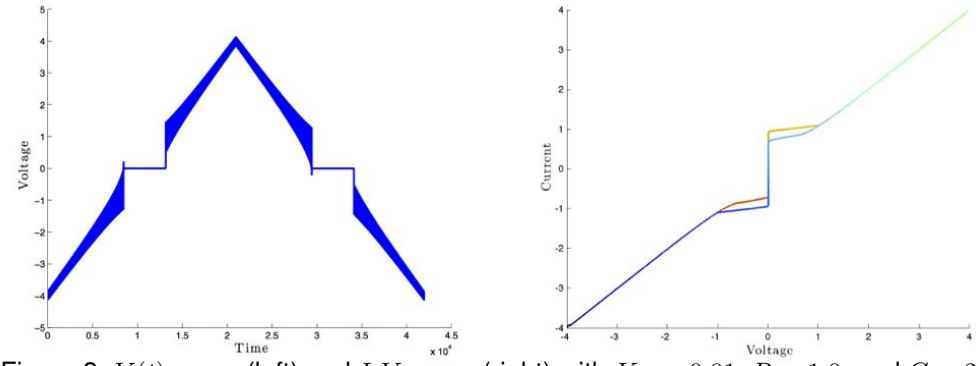

Figure 3. $V(t)$ curve (left) and I-V curve (right) with $K_P = 0.01$, $R = 1.0$, and $C = 2.0$.

When the capacitance is increased further, the oscillation amplitude is decreased further to almost non-existent and the hysteresis is increased, and shown in Figure 4 where $K_P = 0.01$, $R = 1.0$, and $C = 20$. The hysteresis is an undesirable quality in the I-V for the applications in which we are interested. As such, it can be tentatively concluded that a high capacitance is bad.

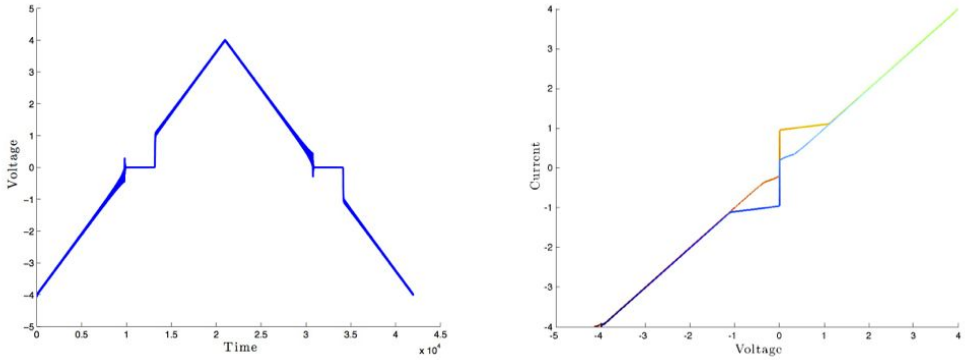

Figure 4. $V(t)$ curve (left) and I-V curve (right) with $K_P = 0.01$, $R = 1.0$, and $C = 20$.

Changing values of R changes τ and β_C since both parameters depend on R, where $\tau \propto R$ and $\beta_C \propto R^2$. Decreasing R below one when β_C is small makes the solution unstable for sufficiently small values of R. This is because the inverse of the matrix used in the modeling becomes practically singular when the value of β_C is very small. The phenomenon is due to modeling instabilities rather than what occurs in a fabricated junction; there are alternate model equations for when $\beta_C = 0$.

For larger β_C, reducing R reduces the hysteresis; see Figure 5 where $K_P = 0.01$, $R = 0.5$, $C = 2.0$, and $\beta_C = 2 \times (0.5)^2 = 0.5$. For these values, the response is approaching the no hysteric ideal solution. There is a slight dampening of the amplitude of oscillations for large negative and positive values of the current and voltage. So, the hysteric effects of a large capacitance can be mitigated, if it is accompanied by a small R.

When non-negligible capacitance is present, increasing the value of R increases the junction hysteresis. The hysteresis is increased faster than when the capacitance is increased due to R being squared in β_C. Figure 6 shows the result of very large hysteresis, where $K_P = 0.01$, $R = 5.0$, $C = 2.0$, and $\beta_C = 2 \times (5.0)^2 = 50$. When the current is negative increasing to positive, the superconductive state is not achieved until the current becomes zero, then the voltage stays zero until the critical current is reached.

From positive to negative current again the response doesn't go into the superconductive state until the current reaches zero, then the voltage stays zero until the negative critical current is reached.

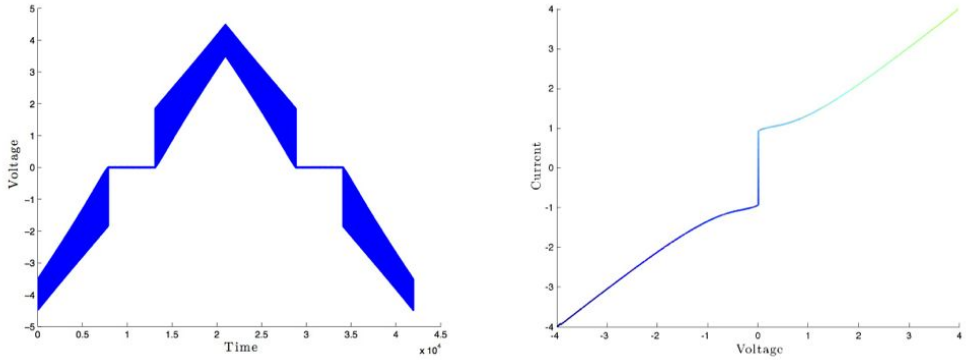

Figure 5. $V(t)$ curve (left) and I-V curve (right) with $K_P = 0.01$, $R = 0.5$, and $C = 2.0$.

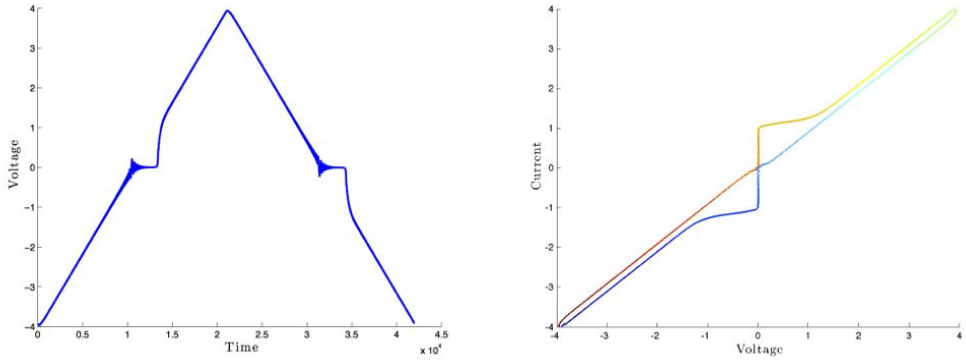

Figure 6. $V(t)$ curve (left) and I-V curve (right) with $K_P = 0.01$, $R = 5.0$, and $C = 2.0$.

For the Josephson junction with $K_P = 1.0$, $R = 1.0$, and $C = 2.0$ modeled in Figure 7, the parameter R has been decreased to the normalized value and the noise temperature has been increased. There is some hysteresis present since $C = 2.0$, but a reduced amount than in the previous case. The transition point (critical current) and hysteresis are both decreased. There are much greater amplitude oscillations for $K_P = 1.0$, especially while in the superconductive state, when compared with all the other examples so far.

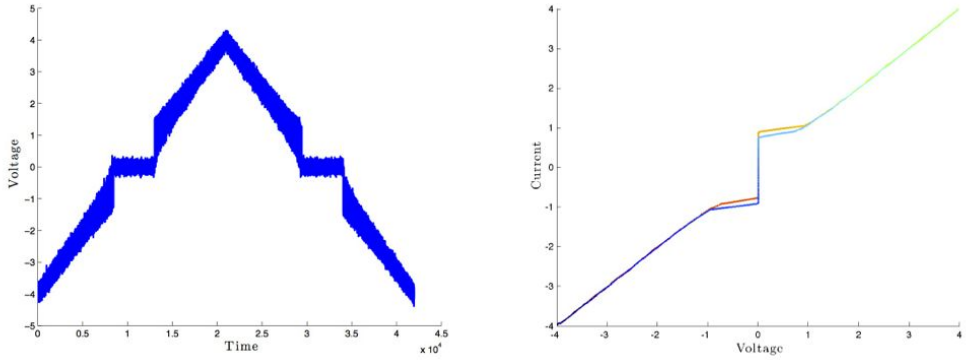

Figure 7. $V(t)$ curve (left) and I-V curve (right) with $K_P = 1.0$, $R = 1.0$, and $C = 2.0$.

If we plot the previous example where $K_P = 1$ with the example from above with the same parameters except with $K_P = 0.01$, and zoom in to the positive current hysteresis loop we get the plots in Figure

8. Black is the warmer temperature. It can be seen clearly that while the hysteresis decreases, the critical current also decreases.

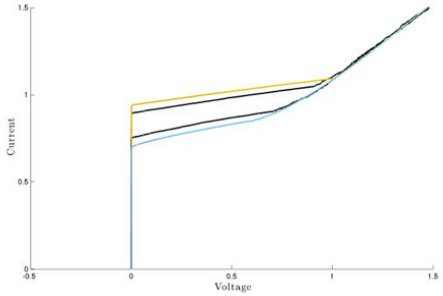

Figure 8. I-V curve (right) with $R = 1.0$, $C = 2.0$, and $K_P = 1.0$ (black), $K_P = 0.01$ (colored).

Finally, for much larger temperatures, the superconductive state disappears completely. Figure 9 has $K_P = 10.0$, $R = 1.0$, and $C = 2.0$. Even when the current is zero, there is sufficient temperature noise to keep the junction in the normal state. Now that we have explored the dynamics of the basic building block of SQUID arrays we will move on to a single SQUID, which is a ring of superconducting materials with two Josephson junctions placed symmetrically across from each other.

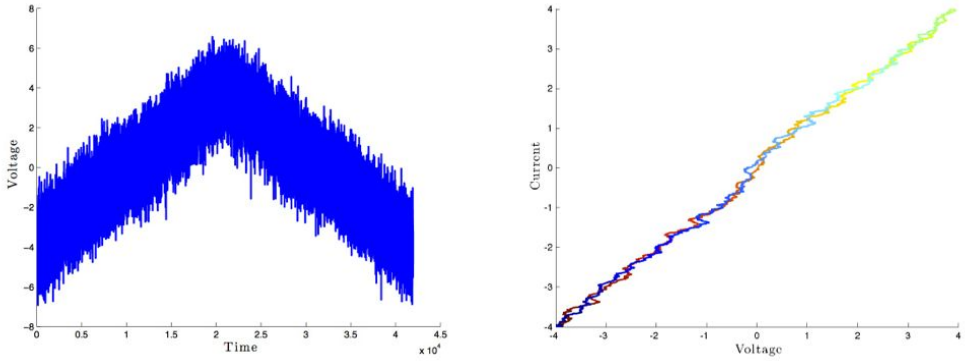

Figure 9. $V(t)$ curve (left) and I-V curve (right) with $K_P = 1.0$, $R = 10$, and $C = 2.0$.

3. SINGLE DC SQUID

In this section we examine the effects of the capacitance, temperature, and resistance of two junctions contained in a ring of superconductive material, commonly called a DC Superconducting Quantum Interference Device or (SQUID). Modeling of the dynamics of the single DC SQUID and DC bi-SQUID, as well as DC SQUID and DC bi-SQUID arrays in both one and two dimensions, without temperature noise or the capacitance terms can be found in [16].

3.1 SYSTEM OF EQUATIONS FOR A SINGLE SQUID

Figure 10 is the schematic diagram of a single DC SQUID.

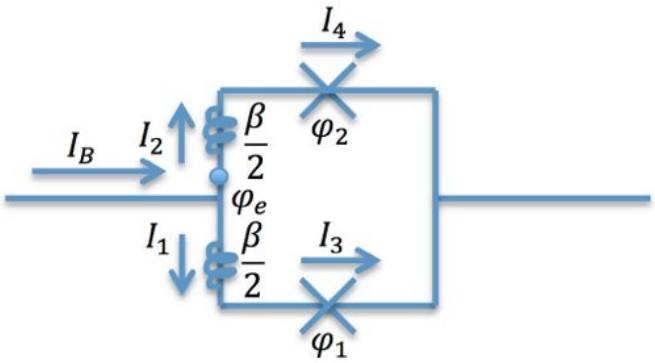

Figure 10. Single DC SQUID schematic.

If we write out the current and phase relationships in the schematics, we get the following six equations:

$$\begin{aligned} i &= \frac{I}{I_0}, \qquad i_1 = i_3, \qquad i_2 = i_4, \qquad i_B = i_1 + i_2 \\ i_3 &= \beta_C \frac{d^2\varphi_1}{d\tau^2} + \frac{d\varphi_1}{d\tau} + i_{c1}\sin\varphi_1 - \frac{2e\kappa_B T}{I_0\hbar} 2\delta(\tau - \tau') \\ i_4 &= \beta_C \frac{d^2\varphi_2}{d\tau^2} + \frac{d\varphi_2}{d\tau} + i_{c2}\sin\varphi_2 - \frac{2e\kappa_B T}{I_0\hbar} 2\delta(\tau - \tau'). \end{aligned}$$

Around the SQUID, there is the relation

$$\varphi_1 + \frac{\beta}{2} i_1 = \varphi_e + \varphi_2 + \frac{\beta}{2} i_2. \tag{2}$$

To get an equation for the first junction, we substitute $i_2 = i_B - i_1$ into Equation (2):

$$\frac{\beta}{2} i_1 = \varphi_e + \varphi_2 - \varphi_1 + \frac{\beta}{2}(i_B - i_1).$$

Rearranging gives

$$\begin{aligned} \beta i_1 &= \frac{\beta}{2} i_B + \varphi_e + \varphi_2 - \varphi_1 \\ i_1 &= \frac{i_B}{2} + \frac{1}{\beta}(\varphi_e + \varphi_2 - \varphi_1). \end{aligned}$$

Substituting $i_1 = i_3$ and then $i_3 = \beta_C \dfrac{d^2\varphi_1}{d\tau^2} + \dfrac{d\varphi_1}{d\tau} + i_{c1}\sin\varphi_1 - \dfrac{2e\kappa_B T}{I_0\hbar}2\delta(\tau - \tau')$ yields

$$\beta_C \frac{d^2\varphi_1}{d\tau^2} + \frac{d\varphi_1}{d\tau} + i_{c1}\sin\varphi_1 - \frac{2e\kappa_B T}{I_0\hbar}2\delta(\tau - \tau') = \frac{i_B}{2} + \frac{1}{\beta}(\varphi_e + \varphi_2 - \varphi_1)$$
$$\beta_C \frac{d^2\varphi_1}{d\tau^2} + \frac{d\varphi_1}{d\tau} = \frac{i_B}{2} + \frac{1}{\beta}(\varphi_e + \varphi_2 - \varphi_1) - i_{c1}\sin\varphi_1 + \frac{2e\kappa_B T}{I_0\hbar}2\delta(\tau - \tau').$$

Similarly, we can substitute $i_1 = i_B - i_2$ into Equation (2) to find a second governing equation

$$\frac{\beta}{2}(i_B - i_2) = \varphi_e + \varphi_2 - \varphi_1 + \frac{\beta}{2}i_2.$$

Rearranging gives

$$\begin{aligned} -\beta i_2 &= -\frac{\beta}{2}i_B + \varphi_e + \varphi_2 - \varphi_1 \\ i_2 &= \frac{i_B}{2} - \frac{1}{\beta}(\varphi_e + \varphi_2 - \varphi_1). \end{aligned}$$

Substituting $i_2 = i_4$ and then $i_4 = \beta_C \dfrac{d^2\varphi_2}{d\tau^2} + \dfrac{d\varphi_2}{d\tau} + i_{c2}\sin\varphi_2 - \dfrac{2e\kappa_B T}{I_0\hbar}2\delta(\tau - \tau')$ yields

$$\beta_C \frac{d^2\varphi_2}{d\tau^2} + \frac{d\varphi_2}{d\tau} + i_{c2}\sin\varphi_2 - \frac{2e\kappa_B T}{I_0\hbar}2\delta(\tau - \tau') = \frac{i_B}{2} - \frac{1}{\beta}(\varphi_e + \varphi_2 - \varphi_1)$$
$$\beta_C \frac{d^2\varphi_2}{d\tau^2} + \frac{d\varphi_2}{d\tau} = \frac{i_B}{2} - \frac{1}{\beta}(\varphi_e + \varphi_2 - \varphi_1) - i_{c2}\sin\varphi_2 + \frac{2e\kappa_B T}{I_0\hbar}2\delta(\tau - \tau'),$$

where φ_1 and φ_2 are the phases across each of the Josephson junctions, β is the normalized inductance and $\varphi_e = 2\pi a x_e$. The parameter $x_e = \dfrac{B_e}{\Phi_0}$ is the normalized external magnetic flux per unit area, and a is the SQUID area. We use the approximate assumption that $a = \beta$.

These two second-order differential equations can be written as a system of four first-order ODEs:

$$\begin{aligned} \frac{d\varphi_1}{d\tau} &= v_1 \\ \beta_C \frac{dv_1}{d\tau} &= \frac{i_B}{2} + \frac{1}{\beta}(\varphi_e + \varphi_2 - \varphi_1) - i_{c1}\sin\varphi_1 - v_1 + \frac{2e\kappa_B T}{I_0\hbar}2\delta(\tau - \tau') \\ \frac{d\varphi_2}{d\tau} &= v_2 \\ \beta_C \frac{dv_2}{d\tau} &= \frac{i_B}{2} - \frac{1}{\beta}(\varphi_e + \varphi_2 - \varphi_1) - i_{c2}\sin\varphi_2 - v_2 + \frac{2e\kappa_B T}{I_0\hbar}2\delta(\tau - \tau'). \end{aligned} \tag{3}$$

3.2 IMAGES FOR A SINGLE SQUID

We integrate the system of equation in Equation (3), varying the bias current over time, then varying the external magnetic field over time. Figure 11 shows the resulting four plots with an ideal response. Here, $K_P = 0.01$, $R = 1.0$, $C = 0.1$, $x_e = 0$, and $\beta = 1.0$ for the top two images, and $K_P = 0.01$, $R = 1.0$, $C = 0.1$, $i_B = 2.0$, and $\beta = 1.0$ for the bottom two images. The top two images are basically the same as the first case for the single junction, but now there are two junctions, we vary i_B from -10.0

to 10.0 and back to -10.0. The bottom two images are the voltage over time and the average voltage response when sweeping over the external magnetic field from -5.0 to 5.0 and back to -5.0.

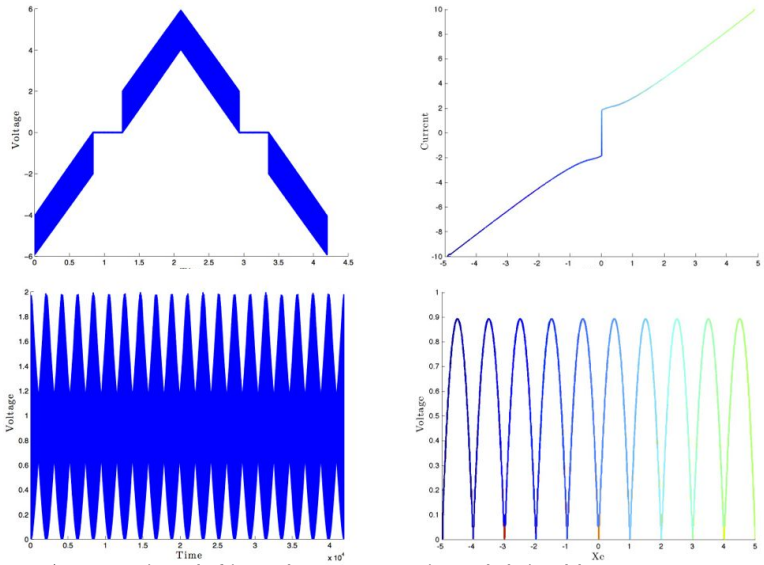

Figure 11. $V(I_B, t)$ curve (top left) and I-V curve (top right) with $K_P = 0.01$, $R = 1.0$, $C = 0.1$, $x_e = 0$, and $\beta = 1.0$. $V(x_e, t)$ curve (bottom left) and $V(x_e)$ curve (bottom right) with $K_P = 0.01$, $R = 1.0$, $C = 0.1$, $i_B = 2.0$, and $\beta = 1.0$.

For the second simulation presented in Figure 12, we increased the capacitance to $C = 2.0$, while keeping the other values the same ($K_P = 0.01$, $R = 1.0$, $x_e = 0$, and $\beta = 1.0$ for the top two images, and $K_P = 0.01$, $R = 1.0$, $i_B = 2.0$, and $\beta = 1.0$ for the bottom). The hysteretic behavior is now present in the I-Vcurve. The presence of hysteresis completely destroys the SQUID average voltage response. While it is still oscillatory, it looses all of its range in voltage. Instead of stretching from 0 to 0.9, it only oscillates between 0.8 and 0.9. This negatively impacts sensing signals since we want the largest voltage swing possible.

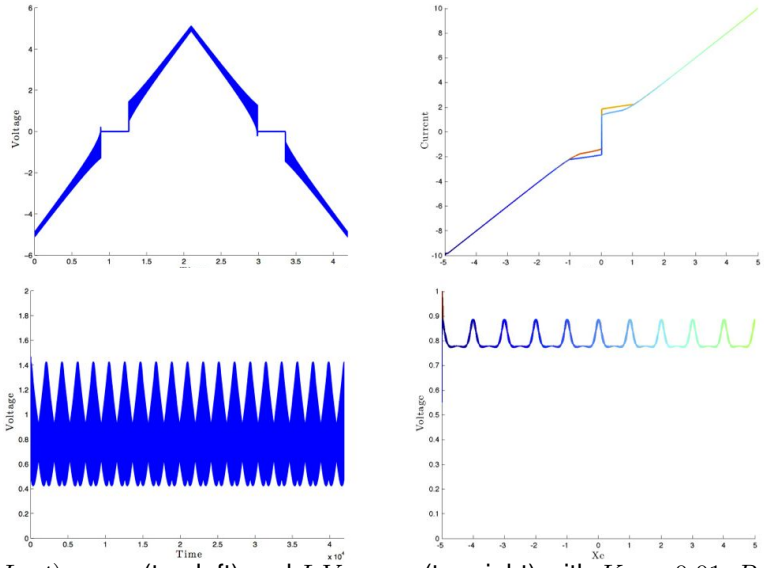

Figure 12. $V(I_B, t)$ curve (top left) and I-V curve (top right) with $K_P = 0.01$, $R = 1.0$, $C = 2.0$, $x_e = 0$, and $\beta = 1.0$. $V(x_e, t)$ curve (bottom left) and $V(x_e)$ curve (bottom right) with $K_P = 0.01$, $R = 1.0$, $C = 2.0$, $i_B = 2.0$, and $\beta = 1.0$.

If we decrease the bias current to be closer to the critical current of the inner part of the hysteric loop on the I-Vcurve ($i_B = 1.55$) then we again get a larger range from 0 to 0.65, but it is far from ideal and there is a large amount of hysteresis present. The other parameters in Figure 13 are $K_P = 0.01$, $R = 1.0$, and $C = 2.0$.

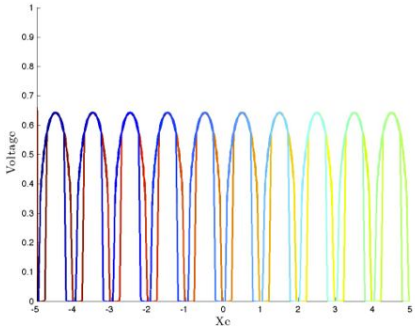

Figure 13. $V(x_e)$ curve with $K_P = 0.01$, $R = 1.0$, $C = 2.0$, $i_B = 1.55$, and $\beta = 1.0$.

For an even larger value of the capacitance ($C = 20$), the average voltage response is non-oscillatory and is a constant line at $V(x_e) = 1$ (see Figure 14).

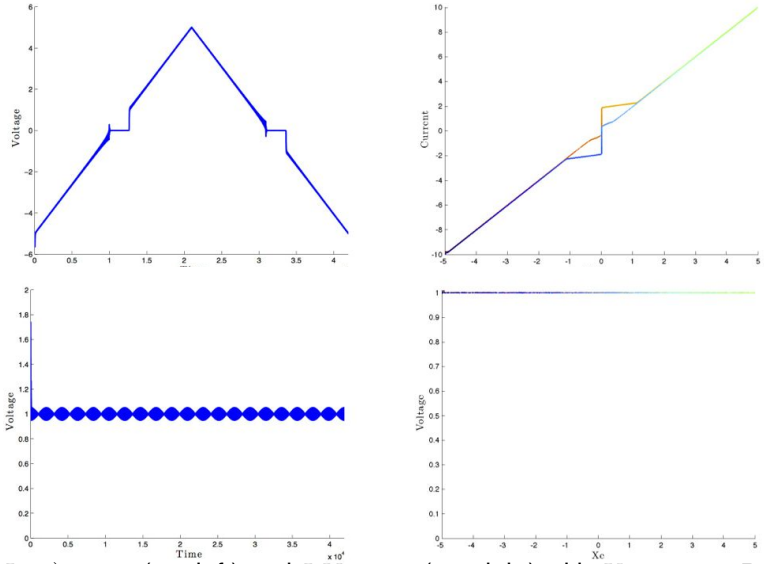

Figure 14. $V(I_B, t)$ curve (top left) and I-V curve (top right) with $K_P = 0.01$, $R = 1.0$, $C = 20$, $x_e = 0$, and $\beta = 1.0$. $V(x_e, t)$ curve (bottom left) and $V(x_e)$ curve (bottom right) with $K_P = 0.01$, $R = 1.0$, $C = 20$, $i_B = 2.0$, and $\beta = 1.0$.

If we go back to capacitance $C = 2.0$, while decreasing the resistance ($R = 0.5$) with the other values remaining the same ($K_P = 0.01$, $x_e = 0$, and $\beta = 1.0$ for the top two images, and $K_P = 0.01$, $i_B = 2.0$, and $\beta = 1.0$ for the bottom), then we restore the original average voltage response (see Figure 15). Some damping is still seen in the voltage over time response for the I-V curve simulation; however, it doesn't seem to impact the average voltage response curve. This is good because it means if there is an unavoidable amount of hysteresis caused by a capacitance, then the response can be improved by decreasing the junction normal resistance. Since $R \propto C^2$, while we simulated the response we didn't include any results here because it looked very similar to Figure 14. The average voltage response was completely destroyed and there was hysteresis in the I-V curve.

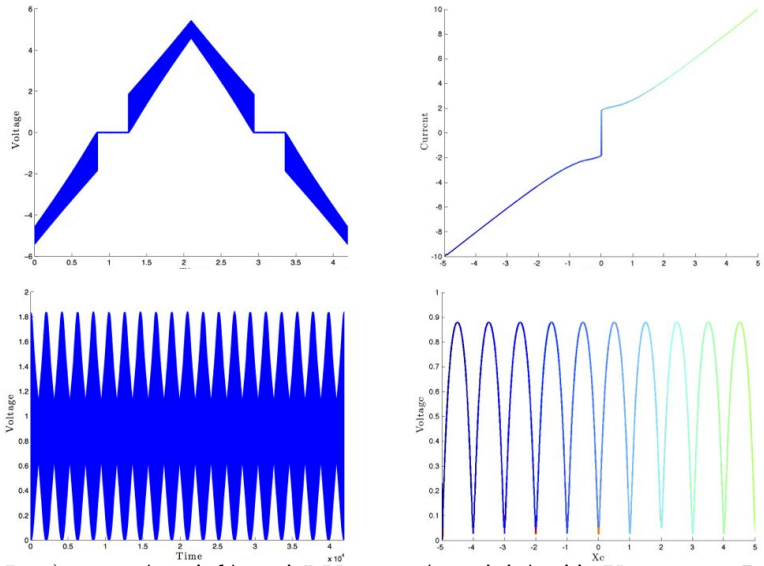

Figure 15. $V(I_B, t)$ curve (top left) and I-V curve (top right) with $K_P = 0.01$, $R = 0.5$, $C = 2.0$, $x_e = 0$, and $\beta = 1.0$. $V(x_e, t)$ curve (bottom left) and $V(x_e)$ curve (bottom right) with $K_P = 0.01$, $R = 0.5$, $C = 2.0$, $i_B = 2.0$, and $\beta = 1.0$.

Next, to see if increasing the noise temperature improves the average voltage response, we set $K_P = 1.0$ and returned to the case where $C = 2.0$, $R = 1.0$, $x_e = 0$, and $\beta = 1.0$ for the top two images of Figure 16, and $C = 2.0$, $R = 1.0$, $i_B = 2.0$, and $\beta = 1.0$ for the bottom. The hysteresis is reduced slightly in the I-Vcurve, but improvement in the average voltage response was minor. With these simulations, we conclude that capacitance is bad at almost any amount, and care should be taken to ensure there is as little as possible present.

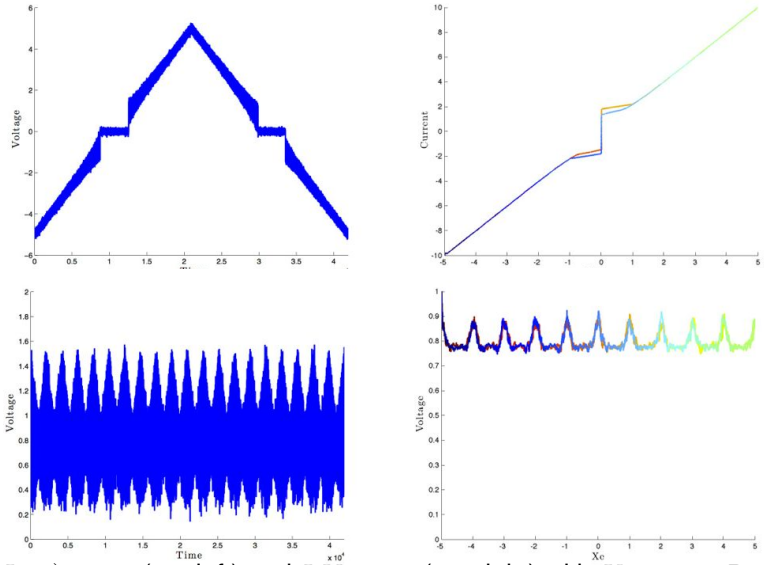

Figure 16. $V(I_B, t)$ curve (top left) and I-V curve (top right) with $K_P = 1.0$, $R = 1.0$, $C = 2.0$, $x_e = 0$, and $\beta = 1.0$. $V(x_e, t)$ curve (bottom left) and $V(x_e)$ curve (bottom right) with $K_P = 1.0$, $R = 1.0$, $C = 2.0$, $i_B = 2.0$, and $\beta = 1.0$.

To see the effects of the noise temperature on a desirable average voltage response, we set $K_P = 1.0$ with $C = 0.1$, $R = 1.0$, $x_e = 0$, and $\beta = 1.0$ for the top two images in Figure 17, and $C = 0.1$, $K_P = 1.0$,

$R = 1.0$, $i_B = 2.0$, and $\beta = 1.0$ for the bottom. There is not much change in the I-V behavior, and while the $V(x_e)$ curve is rougher, the overall shape was maintained.

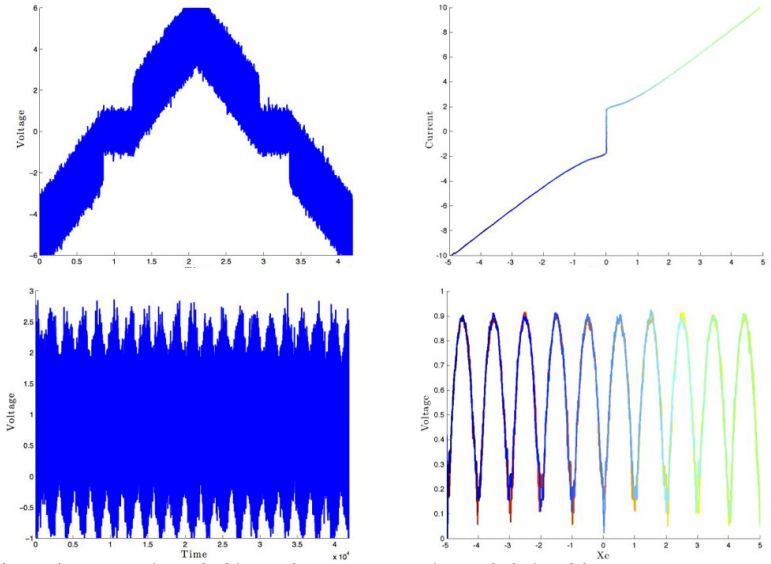

Figure 17. $V(I_B, t)$ curve (top left) and I-V curve (top right) with $K_P = 1.0$, $R = 1.0$, $C = 0.1$, $x_e = 0$, and $\beta = 1.0$. $V(x_e, t)$ curve (bottom left) and $V(x_e)$ curve (bottom right) with $K_P = 1.0$, $R = 1.0$, $C = 0.1$, $i_B = 2.0$, and $\beta = 1.0$.

The last simulation we performed for a single SQUID is a case that could be considered realistic (see Figure 18). There was some capacitance ($C = 0.5$), the resistance had been reduced slightly ($R = 0.9$), and there was some noise from the temperature ($K_P = 0.2$). The other parameters are $x_e = 0$, $\beta = 1.0$ for the top two images, and $i_B = 2.0$, $\beta = 1.0$ for the bottom. Here, the noise is low enough to not affect the average voltage response or the I-V curve much. In addition, the capacitance is offset by the lowered resistance.

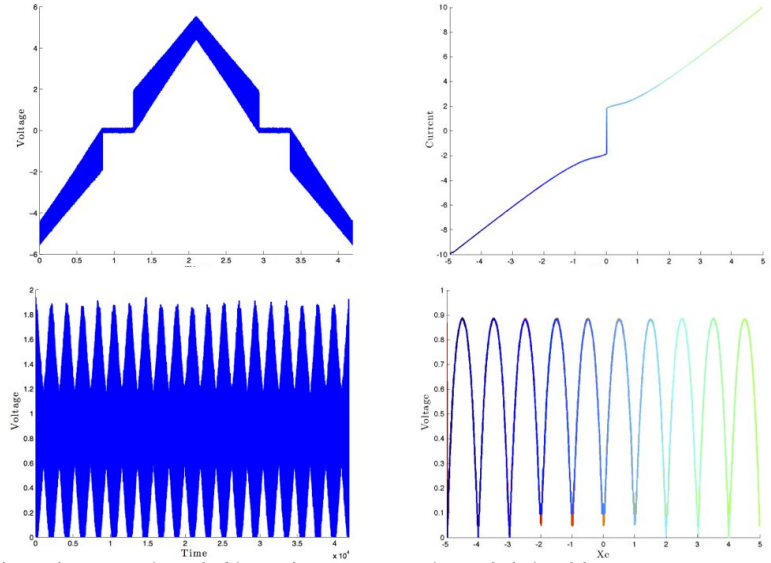

Figure 18. $V(I_B, t)$ curve (top left) and I-V curve (top right) with $K_P = 1.0$, $R = 1.0$, $C = 0.1$, $x_e = 0$, and $\beta = 1.0$. $V(x_e, t)$ curve (bottom left) and $V(x_e)$ curve (bottom right) with $K_P = 1.0$, $R = 1.0$, $C = 0.1$, $i_B = 2.0$, and $\beta = 1.0$.

4. SINGLE DC BI-SQUID

For our study we are interested in the effects of having two ideal junctions around the loop of a bi-SQUID and using a different material and/or method on the bisecting Josephson junction. The previous sections have explored the effects of temperature, capacitance and resistance on the basic building blocks of a bi-SQUID, the single Josephson junction and the single DC SQUID. In this section we will explore the single DC bi-SQUID with the additional terms only on the third junction in the same manner. First we derive the phase equations.

4.1 DERIVATION OF EQUATIONS

Figure 19 is a schematic diagram of a single DC bi-SQUID.

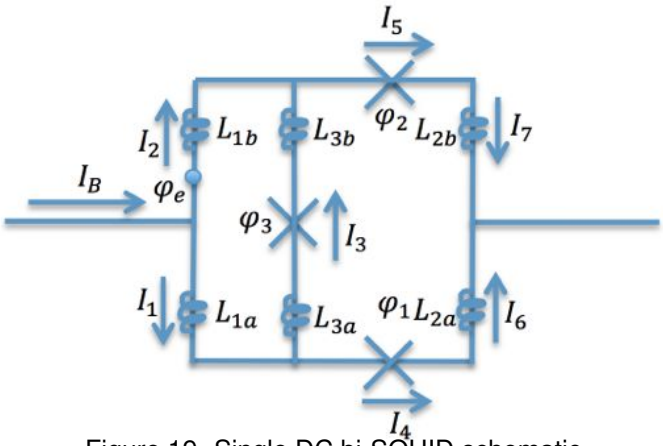

Figure 19. Single DC bi-SQUID schematic.

Using Kirchoff's current law, we get the following six current-phase relations:

$$\begin{aligned} i_3 &= \beta_C \frac{d^2\varphi_3}{d\tau^2} + \frac{d\varphi_3}{d\tau} + i_{c3}\sin\varphi_3 - \frac{2e\kappa_B T}{I_0\hbar} 2\delta(\tau - \tau') \\ i_4 &= \frac{d\varphi_1}{d\tau} + i_{c1}\sin\varphi_1, \qquad i_5 = \frac{d\varphi_2}{d\tau} + i_{c2}\sin\varphi_2 \\ i_B &= i_1 + i_2, \qquad i_1 + i_3 = i_4, \qquad i_2 = i_3 + i_5. \end{aligned}$$

Around the bi-SQUID is the relation

$$\varphi_1 + L_{1a}i_1 + L_{2a}i_4 = \varphi_e + \varphi_2 + L_{1b}i_2 + L_{2b}i_5. \tag{4}$$

To get an equation for the first junction, we substitute $i_2 = i_B - i_1$ into Equation (4).

$$\varphi_1 + L_{1a}i_1 + L_{2a}i_4 = \varphi_e + \varphi_2 + L_{1b}(i_B - i_1) + L_{2b}i_5.$$

Rearranging gives

$$(L_{1b} + L_{1a})i_1 - L_{2b}i_5 + L_{2a}i_4 = \varphi_e + \varphi_2 - \varphi_1 + L_{1b}i_B.$$

Substituting $i_1 = i_4 - i_3$ and then $i_3 = \beta_C \frac{d^2\varphi_3}{d\tau^2} + \frac{d\varphi_3}{d\tau} + i_{c3}\sin\varphi_3 - \frac{2e\kappa_B T}{I_0\hbar}2\delta(\tau-\tau')$, $i_4 = \frac{d\varphi_1}{d\tau} + i_{c1}\sin\varphi_1$, and $i_5 = \frac{d\varphi_2}{d\tau} + i_{c2}\sin\varphi_2$ yields

$$\begin{aligned}
&(L_{1b}+L_{1a})\left(\frac{d\varphi_1}{d\tau} + i_{c1}\sin\varphi_1 - \beta_C\frac{d^2\varphi_3}{d\tau^2} - \frac{d\varphi_3}{d\tau} - i_{c3}\sin\varphi_3 + \frac{2e\kappa_B T}{I_0\hbar}2\delta(\tau-\tau')\right)\\
&\quad - L_{2b}\left(\frac{d\varphi_2}{d\tau} + i_{c2}\sin\varphi_2\right) + L_{2a}\left(\frac{d\varphi_1}{d\tau} + i_{c1}\sin\varphi_1\right) = \varphi_e + \varphi_2 - \varphi_1 + L_{1b}i_B\\
&- L_{2b}\frac{d\varphi_2}{d\tau} + (L_{1b}+L_{1a}+L_{2a})\frac{d\varphi_1}{d\tau} - (L_{1b}+L_{1a})\left(\beta_C\frac{d^2\varphi_3}{d\tau^2} + \frac{d\varphi_3}{d\tau}\right)\\
&\quad = L_{1b}i_B + \varphi_e + \varphi_2 - \varphi_1 - (L_{1b}+L_{1a}+L_{2a})i_{c1}\sin\varphi_1\\
&\qquad + (L_{1b}+L_{1a})\left(i_{c3}\sin\varphi_3 - \frac{2e\kappa_B T}{I_0\hbar}2\delta(\tau-\tau')\right) + L_{2b}i_{c2}\sin\varphi_2.
\end{aligned}$$

Similarly, we can substitute $i_1 = i_B - i_2$ into Equation (4) to find a second governing equation

$$\varphi_1 + L_{1a}(i_B - i_2) + L_{2a}i_4 = \varphi_e + \varphi_2 + L_{1b}i_2 + L_{2b}i_5.$$

Rearranging gives

$$L_{2a}i_4 - (L_{1a}+L_{1b})i_2 - L_{2b}i_5 = \varphi_e + \varphi_2 - \varphi_1 - L_{1a}i_B.$$

Substituting $i_2 = i_3 + i_5$ and then $i_3 = \beta_C \frac{d^2\varphi_3}{d\tau^2} + \frac{d\varphi_3}{d\tau} + i_{c3}\sin\varphi_3 - \frac{2e\kappa_B T}{I_0\hbar}2\delta(\tau-\tau')$, $i_4 = \frac{d\varphi_1}{d\tau} + i_{c1}\sin\varphi_1$, $i_5 = \frac{d\varphi_2}{d\tau} + i_{c2}\sin\varphi_2$ yields

$$\begin{aligned}
&-(L_{1a}+L_{1b})\left(\beta_C\frac{d^2\varphi_3}{d\tau^2} + \frac{d\varphi_3}{d\tau} + i_{c3}\sin\varphi_3 - \frac{2e\kappa_B T}{I_0\hbar}2\delta(\tau-\tau') + \frac{d\varphi_2}{d\tau} + i_{c2}\sin\varphi_2\right)\\
&\quad + L_{2a}\left(\frac{d\varphi_1}{d\tau} + i_{c1}\sin\varphi_1\right) - L_{2b}\left(\frac{d\varphi_2}{d\tau} + i_{c2}\sin\varphi_2\right) = \varphi_e + \varphi_2 - \varphi_1 - L_{1a}i_B\\
&L_{2a}\frac{d\varphi_1}{d\tau} - (L_{1a}+L_{1b}+L_{2b})\frac{d\varphi_2}{d\tau} - (L_{1a}+L_{1b})\left(\beta_C\frac{d^2\varphi_3}{d\tau^2} + \frac{d\varphi_3}{d\tau}\right)\\
&\quad = -L_{1a}i_B + \varphi_e + \varphi_2 - \varphi_1 + (L_{1a}+L_{1b}+L_{2b})i_{c2}\sin\varphi_2\\
&\qquad + (L_{1a}+L_{1b})\left(i_{c3}\sin\varphi_3 - \frac{2e\kappa_B T}{I_0\hbar}2\delta(\tau-\tau')\right) - L_{2a}i_{c1}\sin\varphi_1.
\end{aligned}$$

For the third junction,

$$\varphi_1 + \varphi_3 + L_{2a}i_4 + (L_3a + L_3b)i_3 = L_{2b}i_5 + \varphi_2.$$

Substituting $i_3 = \beta_C \frac{d^2\varphi_3}{d\tau^2} + \frac{d\varphi_3}{d\tau} + i_{c3}\sin\varphi_3 - \frac{2e\kappa_B T}{I_0\hbar}2\delta(\tau-\tau')$, $i_4 = \frac{d\varphi_1}{d\tau} + i_{c1}\sin\varphi_1$, $i_5 = \frac{d\varphi_2}{d\tau} + i_{c2}\sin\varphi_2$ yields

$$
\begin{aligned}
&(L_3a + L_3b)\left(\beta_C\frac{d^2\varphi_3}{d\tau^2} + \frac{d\varphi_3}{d\tau} + i_{c3}\sin\varphi_3 - \frac{2e\kappa_B T}{I_0\hbar}2\delta(\tau-\tau')\right)\\
&\quad + L_{2a}\left(\frac{d\varphi_1}{d\tau} + i_{c1}\sin\varphi_1\right) - L_{2b}\left(\frac{d\varphi_2}{d\tau} + i_{c2}\sin\varphi_2\right) = \varphi_2 - \varphi_1 - \varphi_3\\
&(L_3a + L_3b)\left(\beta_C\frac{d^2\varphi_3}{d\tau^2} + \frac{d\varphi_3}{d\tau}\right) + L_{2a}\frac{d\varphi_1}{d\tau} - L_{2b}\frac{d\varphi_2}{d\tau} = \varphi_2 - \varphi_1 - \varphi_3\\
&\quad - (L_3a + L_3b)\left(i_{c3}\sin\varphi_3 - \frac{2e\kappa_B T}{I_0\hbar}2\delta(\tau-\tau')\right) - L_{2a}i_{c1}\sin\varphi_1 + L_{2b}i_{c2}\sin\varphi_2.
\end{aligned}
$$

Together, we have a system of three differential equations:

$$
\begin{aligned}
&- L_{2b}\frac{d\varphi_2}{d\tau} + (L_{1b} + L_{1a} + L_{2a})\frac{d\varphi_1}{d\tau} - (L_{1b} + L_{1a})\left(\beta_C\frac{d^2\varphi_3}{d\tau^2} + \frac{d\varphi_3}{d\tau}\right)\\
&\quad = L_{1b}i_B + \varphi_e + \varphi_2 - \varphi_1 - (L_{1b} + L_{1a} + L_{2a})i_{c1}\sin\varphi_1\\
&\qquad + (L_{1b} + L_{1a})\left(i_{c3}\sin\varphi_3 - \frac{2e\kappa_B T}{I_0\hbar}2\delta(\tau-\tau')\right) + L_{2b}i_{c2}\sin\varphi_2.\\
&L_{2a}\frac{d\varphi_1}{d\tau} - (L_{1a} + L_{1b} + L_{2b})\frac{d\varphi_2}{d\tau} - (L_{1a} + L_{1b})\left(\beta_C\frac{d^2\varphi_3}{d\tau^2} + \frac{d\varphi_3}{d\tau}\right)\\
&\quad = -L_{1a}i_B + \varphi_e + \varphi_2 - \varphi_1 + (L_{1a} + L_{1b} + L_{2b})i_{c2}\sin\varphi_2\\
&\qquad + (L_{1a} + L_{1b})\left(i_{c3}\sin\varphi_3 - \frac{2e\kappa_B T}{I_0\hbar}2\delta(\tau-\tau')\right) - L_{2a}i_{c1}\sin\varphi_1\\
&(L_3a + L_3b)\left(\beta_C\frac{d^2\varphi_3}{d\tau^2} + \frac{d\varphi_3}{d\tau}\right) + L_{2a}\frac{d\varphi_1}{d\tau} - L_{2b}\frac{d\varphi_2}{d\tau} = \varphi_2 - \varphi_1 - \varphi_3\\
&\quad - (L_3a + L_3b)\left(i_{c3}\sin\varphi_3 - \frac{2e\kappa_B T}{I_0\hbar}2\delta(\tau-\tau')\right) - L_{2a}i_{c1}\sin\varphi_1 + L_{2b}i_{c2}\sin\varphi_2,
\end{aligned}
$$

where the normalized critical current on the third junction is $i_{c3} = \frac{I_{c3}}{I_0}$, $L = 2\pi\frac{lI_0}{\Phi_0}$ is the normalized inductance and we use the approximate assumption that $a = L_{1a} + L_{1b} + L_{2a} + L_{2b}$.

Splitting the second-order differential equation gives a system of four first-order ODEs:

$$
\begin{aligned}
&- L_{2b}\frac{d\varphi_2}{d\tau} + (L_{1b}+L_{1a}+L_{2a})\frac{d\varphi_1}{d\tau} - (L_{1b}+L_{1a})\beta_C\frac{dv}{d\tau} \\
&\quad = L_{1b}i_B + \varphi_e + \varphi_2 - \varphi_1 - (L_{1b}+L_{1a}+L_{2a})i_{c1}\sin\varphi_1 \\
&\qquad + (L_{1b}+L_{1a})(i_{c3}\sin\varphi_3 + v - \frac{2e\kappa_B T}{I_0\hbar}2\delta(\tau-\tau')) + L_{2b}i_{c2}\sin\varphi_2 \\
&L_{2a}\frac{d\varphi_1}{d\tau} - (L_{1a}+L_{1b}+L_{2b})\frac{d\varphi_2}{d\tau} - (L_{1a}+L_{1b})\beta_C\frac{dv}{d\tau} \\
&\quad = -L_{1a}i_B + \varphi_e + \varphi_2 - \varphi_1 + (L_{1a}+L_{1b}+L_{2b})i_{c2}\sin\varphi_2 \\
&\qquad + (L_{1a}+L_{1b})(i_{c3}\sin\varphi_3 + v - \frac{2e\kappa_B T}{I_0\hbar}2\delta(\tau-\tau')) - L_{2a}i_{c1}\sin\varphi_1 \\
&\frac{d\varphi_3}{d\tau} = v \\
&(L_3a + L_3b)\beta_C\frac{dv}{d\tau} + L_{2a}\frac{d\varphi_1}{d\tau} - L_{2b}\frac{d\varphi_2}{d\tau} \\
&\quad = \varphi_2 - \varphi_1 - \varphi_3 - (L_3a+L_3b)(i_{c3}\sin\varphi_3 + v - \frac{2e\kappa_B T}{I_0\hbar}2\delta(\tau-\tau')) \\
&\qquad - L_{2a}i_{c1}\sin\varphi_1 + L_{2b}i_{c2}\sin\varphi_2. \qquad (5)
\end{aligned}
$$

4.2 SIMULATION RESULTS FOR A SINGLE BI-SQUID

Figure 20 is the first example simulation of Equation (5) with $K_P = 0.01$, $R = 1.0$, $C = 0.1$, $x_e = 0$, and $i_{c3} = 0$. The additional terms of K_P and β_c are only on the third junction of the single DC bi-SQUID. We set the inductances to $L_{la} = L_{1b} = 0.27$, $L_{2a} = L_{2b} = 0.24$, and $L_{3a} = L_{3b} = 0.3$. The first image is the voltage over time as the bias current i_B is varied from -10.0 to 10.0 and back to -10.0 of each of the four differential equations. The second image is the voltage over time of the measured output of the bi-SQUID as the bias current i_B is varied over the same range. The third image is the I-V curve for the bi-SQUID, which is determined by filtering the time-dependent voltage and plotting against the input bias current.

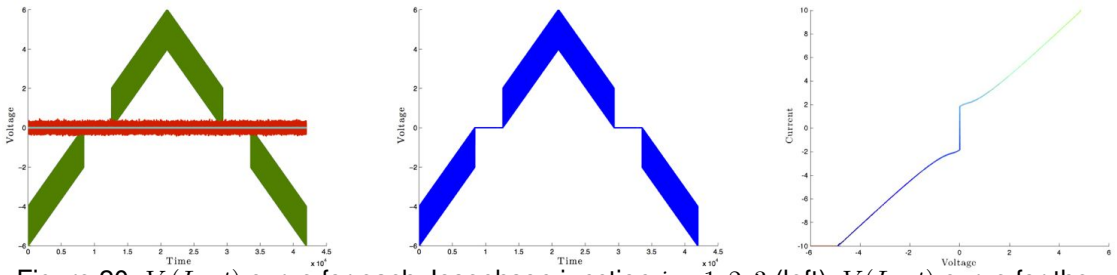

Figure 20. $V_i(I_B, t)$ curve for each Josephson junction $i = 1, 2, 3$ (left), $V(I_B, t)$ curve for the bi-SQUID (middle), and I-V curve (right) with $K_P = 0.01$, $R = 1.0$, $C = 0.1$, $x_e = 0$, and $i_{c3} = 0$.

The three plots in Figure 21 are the average voltage responses of the $K_P = 0.01$, $R = 1.0$, $C = 0.1$, $i_B = 2.0$, and $i_{c3} = 0$. The first image are the voltage over time plots of each differential equation as the external field x_e is varied from -10.0 to 10.0 and back to -10.0. The middle plot is the voltage vs. time output of the bi-SQUID as external field x_e is varied from -5.0 to 5.0 and back to -5.0. The plot on the right side is the $V(x_e)$ curve, which is determined by filtering the voltage over time plot and plotting against the external field.

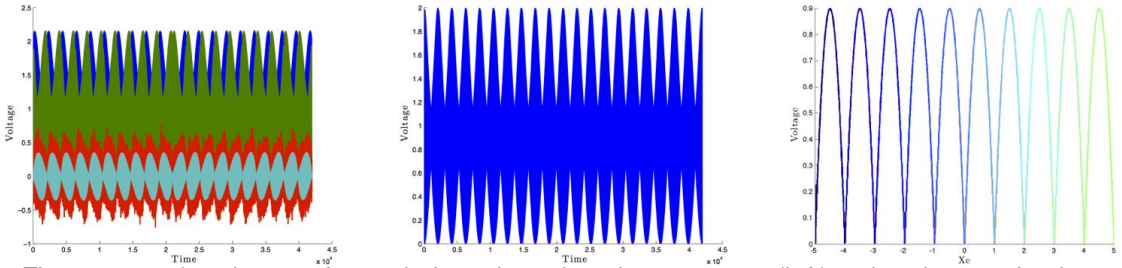

Figure 21. $V_i(x_e, t)$ curve for each Josephson junction $i = 1, 2, 3$ (left), $V(x_e, t)$ curve for the bi-SQUID (middle), and $V(x_e)$ curve (right) with $K_P = 0.01$, $R = 1.0$, $C = 0.1$, $i_B = 2.0$, and $i_{c3} = 0$.

The ideal value of the critical current on the third junction, i_{c3} is 1.0. The average voltage response for a bi-SQUID with $i_{c3} = 1.0$ is shown in Figure 22. This is the value for which $V(x_e)$ is the most linear.

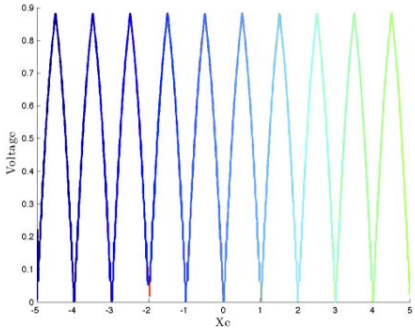

Figure 22. $V(x_e)$ curve (right) with $K_P = 0.01$, $R = 1.0$, $C = 0.1$, $i_B = 2.0$, and $i_{c3} = 1.0$.

Next, we increase the third-junction critical current to see the effects in the I-V and $V(x_e)$ curves (see Figure 23). The top three plots (here $K_P = 0.01$, $R = 1.0$, $C = 0.1$, $x_e = 3.0$, and $i_{c3} = 0$) basically haven't changed. But the $V(x_e)$ plot has definitely changed since hysteresis is present ($K_P = 0.01$, $R = 1.0$, $C = 0.1$, $i_B = 2.0$, and $i_{c3} = 3.0$).

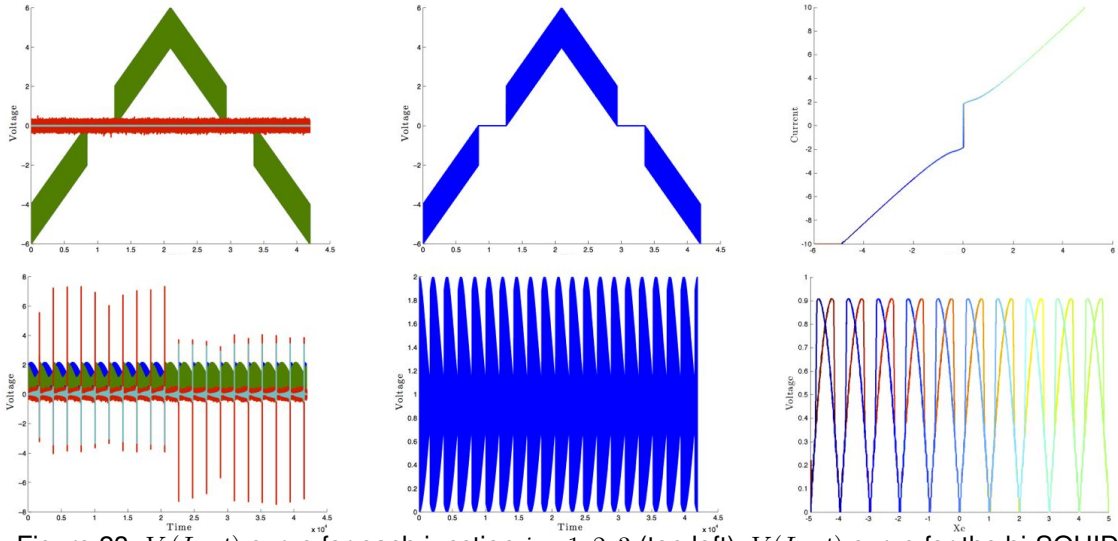

Figure 23. $V_i(I_B, t)$ curve for each junction $i = 1, 2, 3$ (top left), $V(I_B, t)$ curve for the bi-SQUID (top middle), and I-V curve (top right) with $K_P = 0.01$, $R = 1.0$, $C = 0.1$, $x_e = 0$, and $i_{c3} = 3.0$. $V_i(x_e, t)$ curves (bottom left), $V(x_e, t)$ curve (bottom middle), and $V(x_e)$ curve (bottom right) with $K_P = 0.01$, $R = 1.0$, $C = 0.1$, $i_B = 2.0$, and $i_{c3} = 3.0$.

Increasing the capacitance and the resistance of the third junction to $C = 2.0$ and $R = 2.0$ yields the six plots in Figure 24. All other parameters stayed the same as the prior case. While the amplitude in the top left side image and the spikes in bottom left side image of the red and cyan plots (relating to the third junction and the third junction second derivative differential equations) were suppressed, the output I-V and $V(x_e)$ curves were not affected by the increase in capacitance or resistance of the third junction.

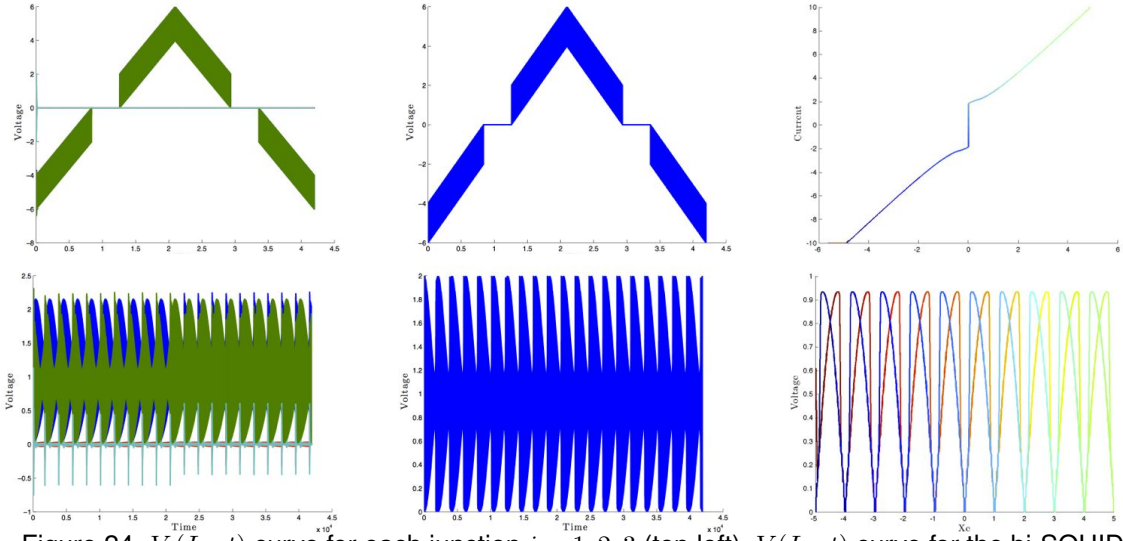

Figure 24. $V_i(I_B, t)$ curve for each junction $i = 1, 2, 3$ (top left), $V(I_B, t)$ curve for the bi-SQUID (top middle), and I-V curve (top right) with $K_P = 0.01$, $R = 2.0$, $C = 2.0$, $x_e = 0$, and $i_{c3} = 3.0$. $V_i(x_e, t)$ curves (bottom left), $V(x_e, t)$ curve (bottom middle), and $V(x_e)$ curve (bottom right) with $K_P = 0.01$, $R = 2.0$, $C = 2.0$, $i_B = 2.0$, and $i_{c3} = 3.0$.

Increasing the capacitance and the resistance further (to $C = 10$ and $R = 10$) results in a smoothing of the I-V curve and destroys the $V(x_e)$ response (see Figure 25). The top left voltage vs. time plot has a large amplitude on the cyan curve, which is transient behavior.

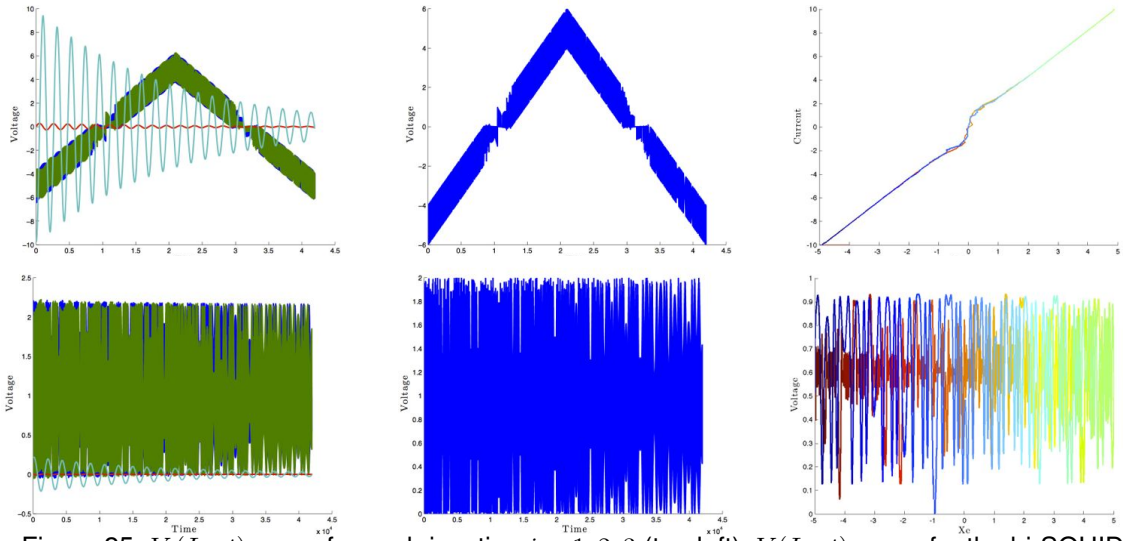

Figure 25. $V_i(I_B, t)$ curve for each junction $i = 1, 2, 3$ (top left), $V(I_B, t)$ curve for the bi-SQUID (top middle), and I-V curve (top right) with $K_P = 0.01$, $R = 10.0$, $C = 10.0$, $x_e = 0$, and $i_{c3} = 3.0$. $V_i(x_e, t)$ curves (bottom left), $V(x_e, t)$ curve (bottom middle), and $V(x_e)$ curve (bottom right) with $K_P = 0.01$, $R = 10.0$, $C = 10.0$, $i_B = 2.0$, and $i_{c3} = 3.0$.

Returning to the case where the top three plots in Figure 26 have $R = 1, C = 0.1, x_e = 0$, and $i_{c3} = 0$, and the bottom three plots have $R = 1, C = 0.1, i_B = 2.0$, and $i_{c3} = 3.0$, but increasing the noise temperature parameter ($K_P = 10$) has almost no effect on the I-V curve. The amplitude of the red curve representing the voltage over time of the third junction second derivative is large in both left side images. This means that the third junction can be a significantly noisier junction than the main two without affecting the I-V curve. The $V(x_e)$ curve is shaggier and looks closer to an average voltage response with a lower i_{c3} value. From this we can determine if the method we are using to create the third junction is noisy, then we want to design it with a higher i_{c3} than we would if it was a theoretically perfect junction.

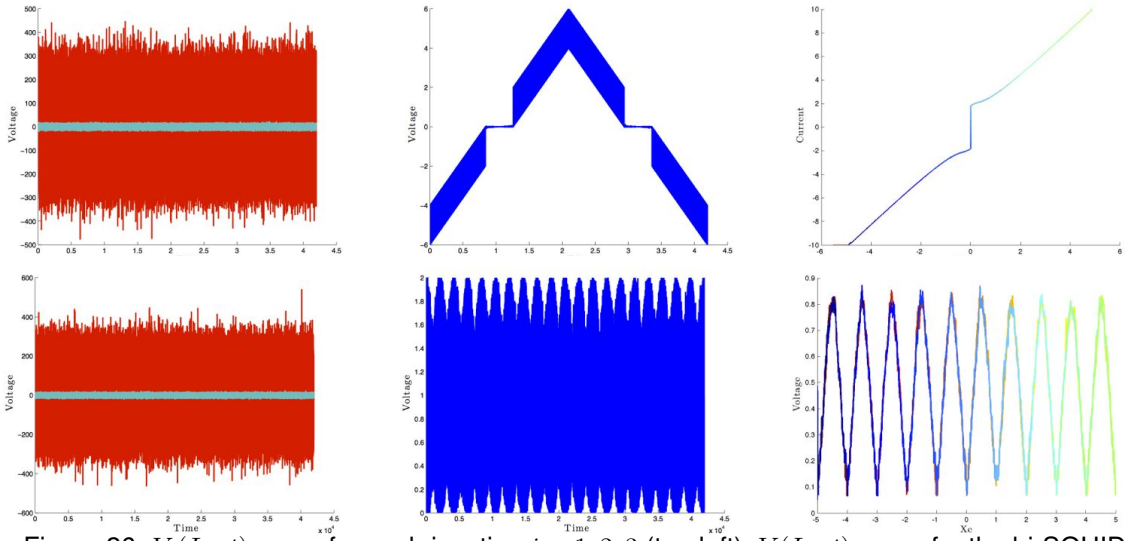

Figure 26. $V_i(I_B, t)$ curve for each junction $i = 1, 2, 3$ (top left), $V(I_B, t)$ curve for the bi-SQUID (top middle), and I-V curve (top right) with $K_P = 10$, $R = 1.0$, $C = 0.1$, $x_e = 0$, and $i_{c3} = 3.0$. $V_i(x_e, t)$ curves (bottom left), $V(x_e, t)$ curve (bottom middle), and $V(x_e)$ curve (bottom right) with $K_P = 10$, $R = 1.0$, $C = 0.1$, $i_B = 2.0$, and $i_{c3} = 3.0$.

Increasing the noise temperature parameter further ($K_P = 100$) makes the I-V curve simply the normal state resistance curve, with no superconducting area ($V = 2I_c$), shown in Figure 27. The $V(x_e)$ curve no longer exhibits oscillatory behaviors. This is most likely due to so much noise on the third junction (probably an unrealistic amount) that it is leaking into the other junctions and driving the whole bi-SQUID normal. There is likely a value of K_P between 10 and 100 for which the third junction is driven normal (i_{c3} to zero), and the dynamics of an array of DC SQUIDs is recovered. More investigation is needed.

Finally, we look at the effects of increasing capacitance and resistance in the presence of thermal noise. The top three images in Figure 28 have $K_P = 5.0$, $R = 1.0$, $C = 0.1$, $i_B = 2.0$, and $i_{c3} = 3.0$, and the bottom three images have $K_P = 5.0$, $R = 2.0$, $C = 2.0$, $i_B = 2.0$, and $i_{c3} = 3.0$. The increase in capacitance and resistance suppresses the noise. Since the noise is suppressed, the effect of higher linearity with larger i_{c3} values is reversed, and the hysteresis reappears.

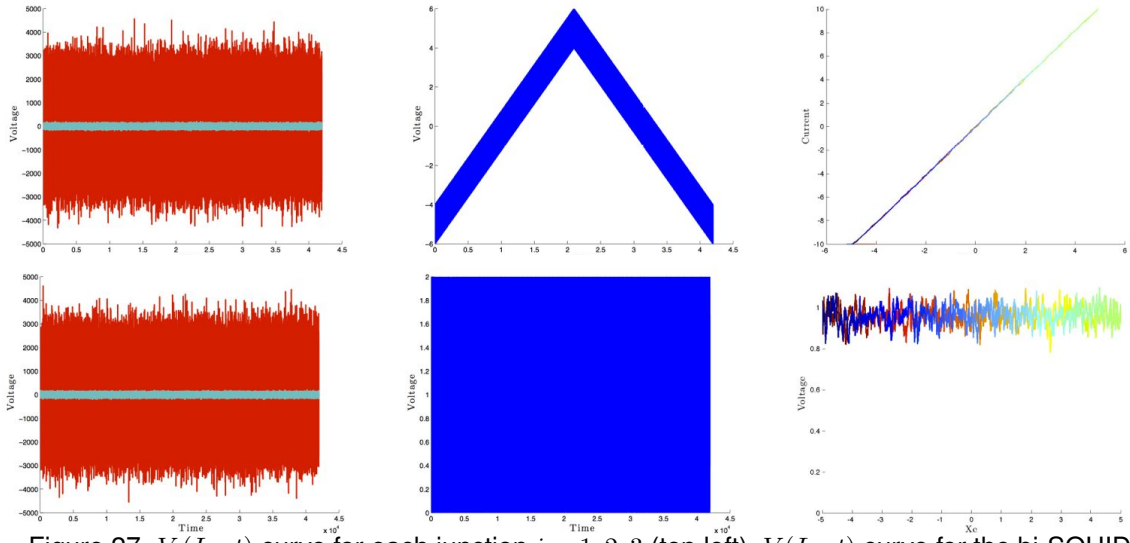

Figure 27. $V_i(I_B, t)$ curve for each junction $i = 1, 2, 3$ (top left), $V(I_B, t)$ curve for the bi-SQUID (top middle), and I-V curve (top right) with $K_P = 100$, $R = 1.0$, $C = 0.1$, $x_e = 0$, and $i_{c3} = 3.0$. $V_i(x_e, t)$ curves (bottom left), $V(x_e, t)$ curve (bottom middle), and $V(x_e)$ curve (bottom right) with $K_P = 100$, $R = 1.0$, $C = 0.1$, $i_B = 2.0$, and $i_{c3} = 3.0$.

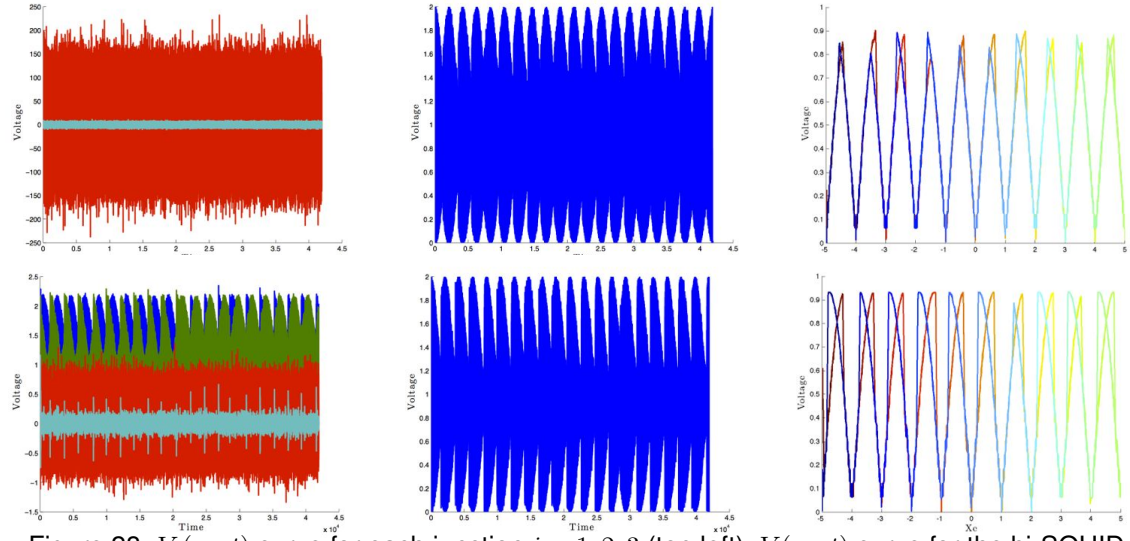

Figure 28. $V_i(x_e, t)$ curve for each junction $i = 1, 2, 3$ (top left), $V(x_e, t)$ curve for the bi-SQUID (top middle), and $V(x_e)$ curve (top right) with $K_P = 5.0$, $R = 1.0$, $C = 0.1$, $i_B = 2.0$, and $i_{c3} = 3.0$. $V_i(x_e, t)$ curves (bottom left), $V(x_e, t)$ curve (bottom middle), and $V(x_e)$ curve (bottom right) with $K_P = 5.0$, $R = 2.0$, $C = 2.0$, $i_B = 2.0$, and $i_{c3} = 3.0$.

5. SERIES BI-SQUID ARRAY

Now that we have an idea of how the single DC bi-SQUID behaves with a different third junction, we explore an array of DC bi-SQUIDs coupled together in a series fashion. The sensor we are designing will not be a single bi-SQUID, but an array of thousands, so it is important to understand the effects when they are coupled together.

5.1 SYSTEM OF EQUATIONS

In Figure 29 we show the schematic diagram for an array of DC bi-SQUIDs coupled in series.

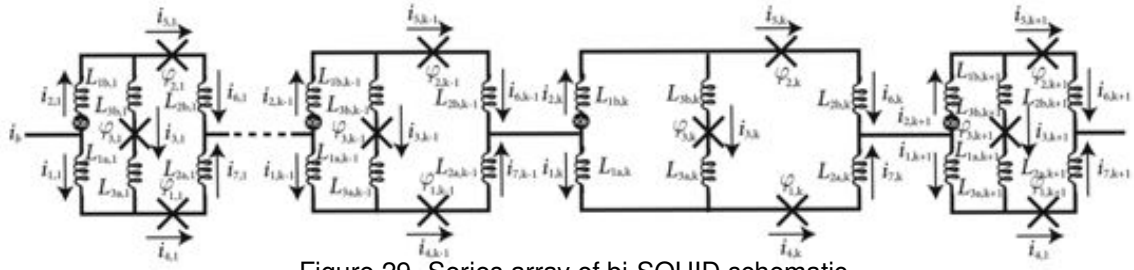

Figure 29. Series array of bi-SQUID schematic.

Since the coupling is in series, we don't need to derive new equations, we can just extend the single bi-SQUID equations to an array of N bi-SQUIDs by including a mutual coupling term of strength M [16]. The system of $4N$ first-order ODEs is

$$
\begin{aligned}
&(L_{1b,k}+L_{1a,k}+L_{2a,k})\frac{d\varphi_{1,k}}{d\tau}-L_{2b,k}\frac{d\varphi_{2,k}}{d\tau}-(L_{1b,k}+L_{1a,k})\beta_{C,k}\frac{dv_k}{d\tau}\\
&\quad=L_{1b,k}i_B+\varphi_{e,k}+\varphi_{2,k}-\varphi_{1,k}-(L_{1b,k}+L_{1a,k}+L_{2a,k})i_{c1,k}\sin\varphi_{1,k}\\
&\qquad+(L_{1b,k}+L_{1a,k})\left(i_{c3,k}\sin\varphi_{3,k}+v_k-\frac{2e\kappa_BT}{I_0\hbar}2\delta_k(\tau-\tau')\right)\\
&\qquad+L_{2b,k}i_{c2,k}\sin\varphi_{2,k}+\sum_{i\neq k}\frac{M}{d_i^3a_i}(\varphi_{1,i}-\varphi_{2,i}-2\pi x_ea_i)\\
&L_2a\frac{d\varphi_{1,k}}{d\tau}-(L_{1a,k}+L_{1b,k}+L_{2b,k})\frac{d\varphi_{2,k}}{d\tau}-(L_{1a,k}+L_{1b,k})\beta_{C,k}\frac{dv_k}{d\tau}\\
&\quad=-L_{1a,k}i_B+\varphi_{e,k}+\varphi_{2,k}-\varphi_{1,k}+(L_{1a,k}+L_{1b,k}+L_{2b,k})i_{c2,k}\sin\varphi_{2,k}\\
&\qquad+(L_{1a,k}+L_{1b,k})\left(i_{c3,k}\sin\varphi_{3,k}+v_k-\frac{2e\kappa_BT}{I_0\hbar}2\delta_k(\tau-\tau')\right)\\
&\qquad-L_{2a,k}i_{c1,k}\sin\varphi_{1,k}+\sum_{i\neq k}\frac{M}{d_i^3a_i}(\varphi_{1,i}-\varphi_{2,i}-2\pi x_ea_i)\\
&\frac{d\varphi_{3,k}}{d\tau}=v_k\\
&L_{2a,k}\frac{d\varphi_{1,k}}{d\tau}-L_{2b,k}\frac{d\varphi_{2,k}}{d\tau}+(L_{3a,k}+L_{3b,k})\beta_{C,k}\frac{dv_k}{d\tau}\\
&\quad=\varphi_{2,k}-\varphi_{1,k}-\varphi_{3,k}-L_{2a,k}i_{c1,k}\sin\varphi_{1,k}+L_{2b,k}i_{c2,k}\sin\varphi_{2,k}\\
&\qquad-(L_{3a,k}+L_{3b,k})\left(i_{c3,k}\sin\varphi_{3,k}+v_k-\frac{2e\kappa_BT}{I_0\hbar}2\delta_k(\tau-\tau')\right),
\end{aligned}
\tag{6}
$$

where $\varphi_{1,k}$, $\varphi_{2,k}$ and $\varphi_{3,k}$ are the phases across the Josephson junction in each of the bi-SQUIDs, $k=1,...,N$.

5.2 SERIES BI-SQUID SIMULATIONS

To start off, we simulate Equation (6) for an ideal array of 50 bi-SQUIDs. This array has small capacitance ($C = 0.1$), small temperature noise ($K_P = 0.01$), resistance of one ($R = 1.0$), and third junction current of one ($i_{c3} = 1$) (see Figure 30). We set the midpoint inductances to $L_{la,k} = L_{1b,k} = 0.27$, $L_{2a,k} = L_{2b,k} = 0.24$, $L_{3a,k} = L_{3b,k} = 0.3$ and vary with a Gaussian distribution along with loop areas between $a = 0.52$ and $a = 1.52$, and use only nearest neighbor coupling with $M = 0.001$. The top left image is the voltage over time of the array as the bias current i_B is varied from -10.0 to 10.0 and back to -10.0 when $x_e = 0$. The top right image is the I-V curve for the array, which is determined by filtering the time dependent voltage and plotting against the input bias current. The bottom left image is the voltage vs. time output of the array as the external field x_e is varied from -5.0 to 5.0 and back to -5.0 when $i_B = 2.0$. The plot on the bottom right is the $V(x_e)$ curve for the array, which is determined by filtering the voltage over time plot and plotting against the external field. The feature we are interested in is the anti-peak around the zero magnetic field. We want the anti-peak to have a large voltage swing and be highly linear for signal detection purposes.

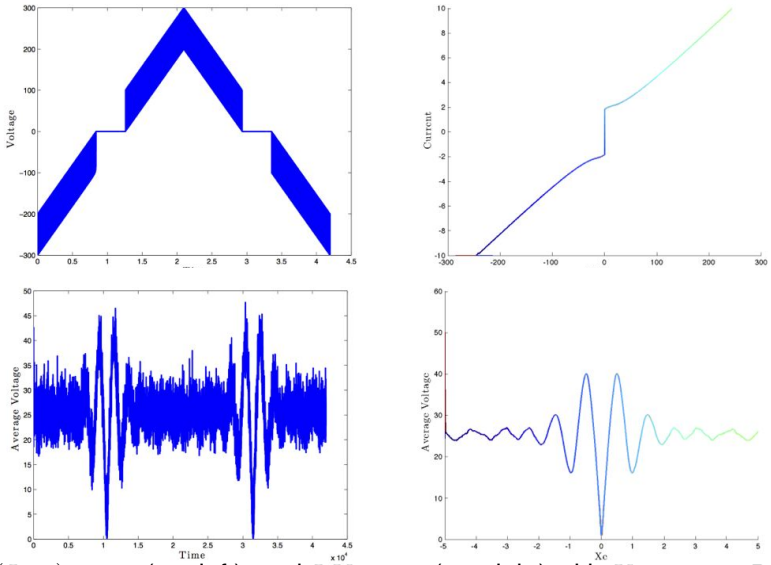

Figure 30. $V(I_B, t)$ curve (top left), and I-V curve (top right) with $K_P = 0.01$, $R = 1.0$, $C = 0.1$, $i_{c3} = 1.0$, $x_e = 0$, $N = 50$, and $M = 0.001$. $V(x_e, t)$ curve (bottom left), and $V(x_e)$ curve (bottom right) with $K_P = 0.01$, $R = 1.0$, $C = 0.1$, $i_{c3} = 1.0$, $i_B = 2.0$, $N = 50$, and $M = 0.001$. The loops have a Gaussian distribution between $a = 0.52$ and $a = 1.52$.

Next we increase the capacitance and the resistance values to $C = 2.0$ and $R = 2.0$ to get the four plots in Figure 31. All other parameters stayed the same as the prior case. The output I-V and $V(x_e)$ curves were not affected by the increase in capacitance or resistance of the third junction. This amount of capacitance and resistance on the third junction does not translate to hysteresis in the I-V. From this we can determine that the main two junctions are the source of the hysteric behaviors.

Increasing the capacitance and resistance further completely destroys the anti-peak as shown in Figure 32, where $C = 10$ and $R = 10$. The I-V curve still shows some structure, but it doesn't contain a segment where there is zero resistance to current. There is still not much hysteresis present, even with this high of a capacitance and resistance on the third junction.

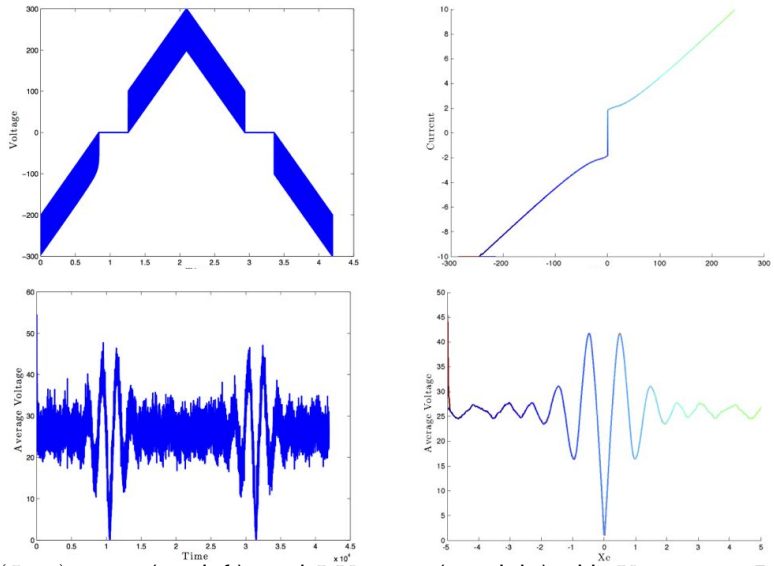

Figure 31. $V(I_B, t)$ curve (top left), and I-V curve (top right) with $K_P = 0.01$, $R = 2.0$, $C = 2.0$, $i_{c3} = 1.0$, $x_e = 0$, $N = 50$, and $M = 0.001$. $V(x_e, t)$ curve (bottom left), and $V(x_e)$ curve (bottom right) with $K_P = 0.01$, $R = 2.0$, $C = 2.0$, $i_{c3} = 1.0$, $i_B = 2.0$, $N = 50$, and $M = 0.001$. The loops have a Gaussian distribution between $a = 0.52$ and $a = 1.52$.

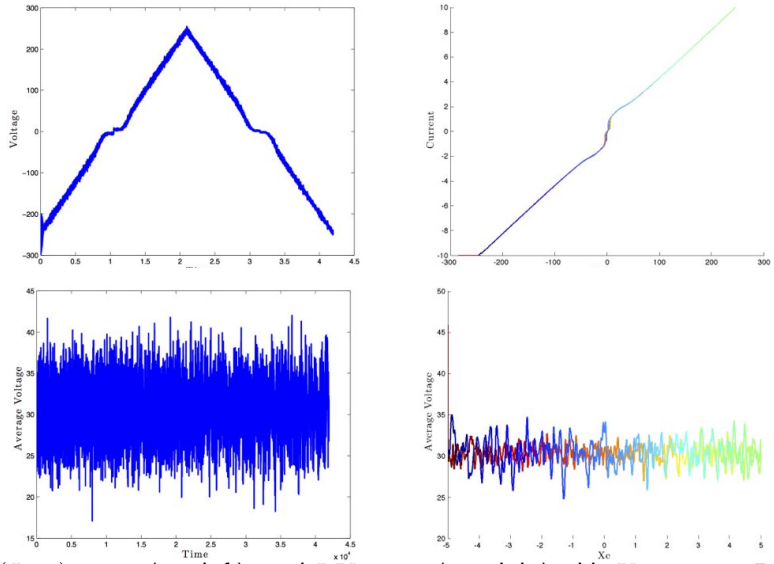

Figure 32. $V(I_B, t)$ curve (top left), and I-V curve (top right) with $K_P = 0.01$, $R = 10$, $C = 10$, $i_{c3} = 1.0$, $x_e = 0$, $N = 50$, and $M = 0.001$. $V(x_e, t)$ curve (bottom left), and $V(x_e)$ curve (bottom right) with $K_P = 0.01$, $R = 10$, $C = 10$, $i_{c3} = 1.0$, $i_B = 2.0$, $N = 50$, and $M = 0.001$. The loops have a Gaussian distribution between $a = 0.52$ and $a = 1.52$.

Now we return to the case where $R = 1.0$, and $C = 0.1$, and increase K_P to 10. The results are in Figure 33. This amount of noise is more prevalent in the voltage over time plots than the final filtered response. The I-V is hardly affected at all. The $V(x_e)$ curve has some loss in voltage swing from 5.0 to 0.0.

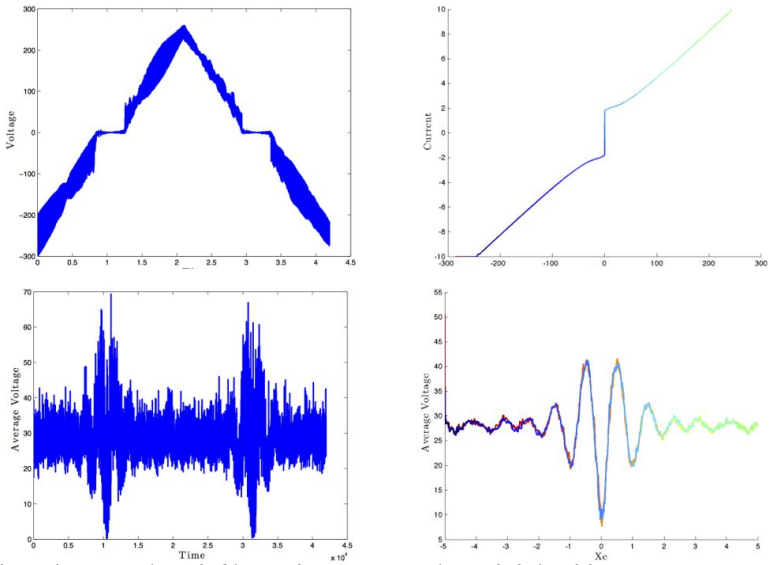

Figure 33. $V(I_B, t)$ curve (top left), and I-V curve (top right) with $K_P = 10$, $R = 1.0$, $C = 0.1$, $i_{c3} = 1.0$, $x_e = 0$, $N = 50$, and $M = 0.001$. $V(x_e, t)$ curve (bottom left), and $V(x_e)$ curve (bottom right) with $K_P = 10$, $R = 1.0$, $C = 0.1$, $i_{c3} = 1.0$, $i_B = 2.0$, $N = 50$, and $M = 0.001$. The loops have a Gaussian distribution between $a = 0.52$ and $a = 1.52$.

If K_P is increased to 100, then the I-V curve is driven normal and the anti-peak disappears completely (see Figure 34). This is the response we would see if the bisecting Josephson junction was not superconducting, while the main two junctions were superconducting. The bi-SQUID array does not just return to simple SQUID array dynamics. As in the case of the single bi-SQUID, this is probably due to the noise on the third junction measuring so incredibly high that it is bleeding into the other junctions and driving the whole array normal. More investigation is needed.

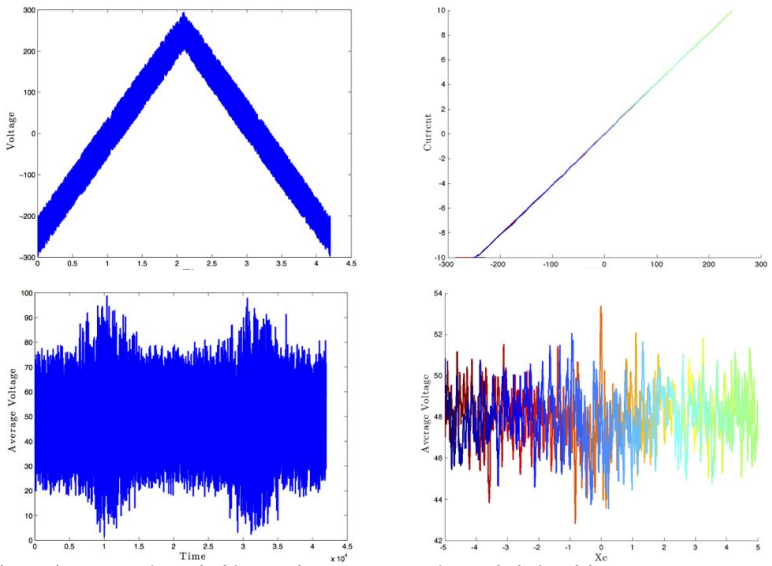

Figure 34. $V(I_B, t)$ curve (top left), and I-V curve (top right) with $K_P = 100$, $R = 1.0$, $C = 0.1$, $i_{c3} = 1.0$, $x_e = 0$, $N = 50$, and $M = 0.001$. $V(x_e, t)$ curve (bottom left), and $V(x_e)$ curve (bottom right) with $K_P = 100$, $R = 1.0$, $C = 0.1$, $i_{c3} = 1.0$, $i_B = 2.0$, $N = 50$, and $M = 0.001$. The loops have a Gaussian distribution between $a = 0.52$ and $a = 1.52$.

The final simulation we ran was to increase all three parameters a little, $K_P = 5.0$, $R = 2.0$, and $C = 2.0$ (see Figure 35). This would be a more realistic situation with a poorly constructed third junction and near perfect main junctions. These values hardly effect the anti-peak of the $V(x_e)$ curve at all. The linearity and voltage swing seems to be retained.

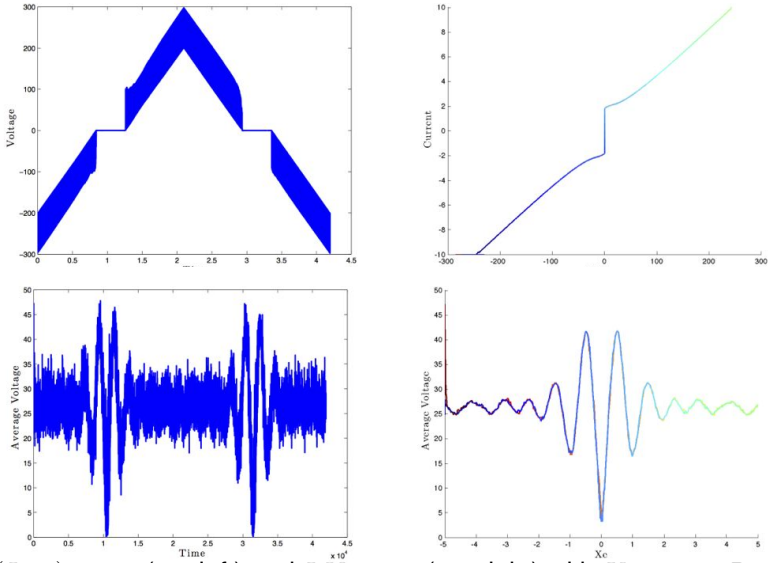

Figure 35. $V(I_B, t)$ curve (top left) and I-V curve (top right) with $K_P = 5.0$, $R = 2.0$, $C = 2.0$, $i_{c3} = 1.0$, $x_e = 0$, $N = 50$, $M = 0.001$. $V(x_e, t)$ curve (bottom left) and $V(x_e)$ curve (bottom right) with $K_P = 5.0$, $R = 2.0$, $C = 2.0$, $i_{c3} = 1.0$, $i_B = 2.0$, $N = 50$, $M = 0.001$. The loops have a Gaussian distribution between $a = 0.52$ and $a = 1.52$.

6. FREQUENCY DEPENDENCE OF A BI-SQUID

We want to explore the effects of frequency dependence on gain and linearity. The frequency dependence can manifest in many areas, for example, the conductivity and the plasma frequency. The conductivity is the inverse of resistance and the plasma frequency depends on distances between the junctions and is dependent on the potential carrier density. Here, we first set critical current of the third junction as frequency dependent for a single bi-SQUID, with schematic as seen in Figure 19.

6.1 SIMPLIFIED EQUATIONS

Without the temperature and capacitance terms, the single bi-SQUIDs equations are

$$\begin{aligned}
(L_1+L_{2a})\frac{d\varphi_1}{d\tau}-L_{2b}\frac{d\varphi_2}{d\tau}-L_1\frac{d\varphi_3}{d\tau} &= \varphi_2-\varphi_1+L_{1b}i_B+2\pi x_e a+L_1 i_{c3}\sin\varphi_3 \\
&\quad +L_{2b}\sin\varphi_2-(L_1+L_{2a})\sin\varphi_1 \\
L_{2a}\frac{d\varphi_1}{d\tau}-(L_1+L_{2b})\frac{d\varphi_2}{d\tau}-L_1\frac{d\varphi_3}{d\tau} &= \varphi_2-\varphi_1-L_{1a}i_B+2\pi x_e a+L_1 i_{c3}\sin\varphi_3 \\
&\quad -L_{2a}\sin\varphi_1+(L_1+L_{2b})\sin\varphi_2 \\
L_{2a}\frac{d\varphi_1}{d\tau}-L_{2b}\frac{d\varphi_2}{d\tau}-L_3\frac{d\varphi_3}{d\tau} &= \varphi_2-\varphi_3-\varphi_1-L_3 i_{c3}\sin\varphi_3 \\
&\quad -L_{2a}\sin\varphi_1+L_{2b}\sin\varphi_2,
\end{aligned}$$

where $L_1 = L_{1a} + L_{1b}$, $L_3 = L_{3a} + L_{3b}$.

The external signal is added to the x_e term in the equations as $A\sin(2\pi f\tau)$, where A is the amplitude and f is the frequency. To simulate the frequency dependence, a Heaviside function is used to change the value of i_{c3}, depending of the incoming signals frequency. Three cases were explored. One was that the response after a certain frequency would act like a traditional SQUID, or $i_{c3} = 0$ for $f > f_c$, where f_c is the cut-off frequency for the Heaviside function. The next was that the third junction line would act like a wire connecting the two sides of the bi-SQUID. We represented this by setting $i_{c3} = 10.0$ for $f > f_c$. The last case explored was the control case, where there was no frequency dependence introduced.

6.2 FREQUENCY SIMULATIONS

The average voltage response of a single SQUID (blue) and single bi-SQUID (green) is shown in Figure 36. These were created by taking the average of the time-dependent voltage response $\frac{\dot{\varphi}_1+\dot{\varphi}_2}{2}$ at a point in x_e. This procedure was done for a range of x_e with $i_B = 2.002$. The average voltage response of a single bi-SQUID is much more linear than an single SQUID. This is important for signal detection, since the greater the linearity, the smaller the spurious signals.

To find the output and spurious signal strength, the time-dependent voltage was determined with an input signal present, then a power spectral density was taken to determine the output signal strength; see an example at 300 MHz in Figure 37. This was done for a number of frequencies in the 30 MHz and 3 GHz range. For each of the three cases simulated, the normalized critical current of the third junction was equal to 1.0 until the cut-off frequency.

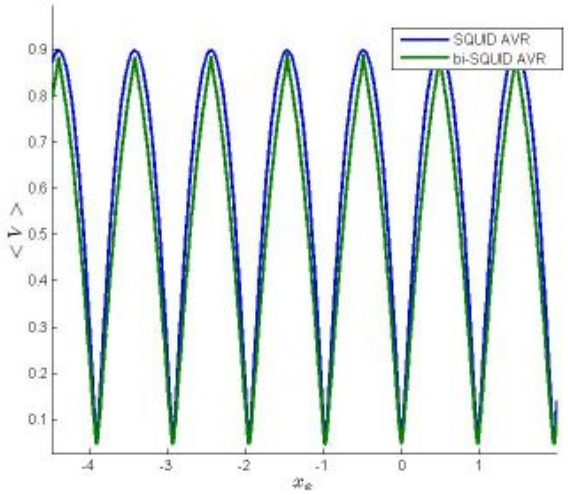

Figure 36. Average voltage response of a single SQUID (blue) and a single bi-SQUID (green).

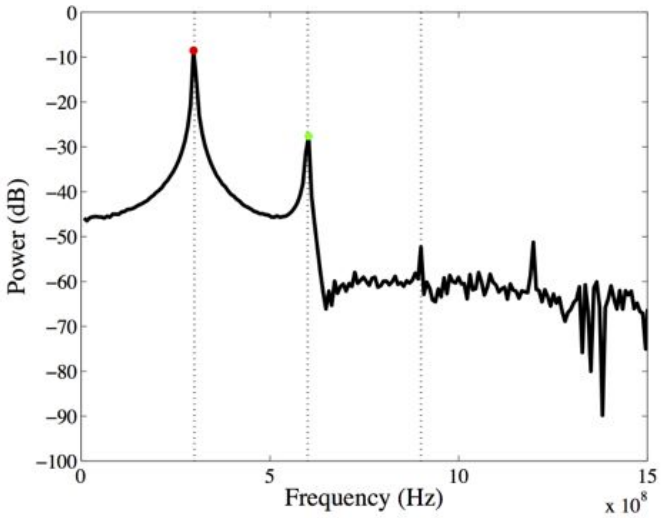

Figure 37. Power spectral density plot for $i_{c3} = 1.0$, and $f = 300$ Mhz.

The output signal power determined from the simulations of a frequency input between 30 MHz and 3 GHz with a cut-off frequency $F_c = 500$ MHz for a signal with amplitude 0.25 is shown in Figure 38. These plots were created with $x_e = 0.25$, $i_B = 2.00$. The control case, where there was no change in i_{c3}, and the case where the bi-SQUID because a regular SQUID have no difference is output signal power; however, the case where the critical current increases to 10.0 the output signal power drops by more than 20 dB, to the level of the spurious signals in Figure 39.

The largest spurious signals can be seen in Figure 39. The largest spur increased in power when the critical current became 0.0 after the cut off frequency. This is expected due to the difference in linearity in the $V(x_e)$ between the SQUID response and bi-SQUID response. For the case when the critical current increased to 10.0 there were no spurs present so the response is basically at the noise floor of the system and the output signal power itself was the strength of a spur for a bi-SQUID or SQUID.

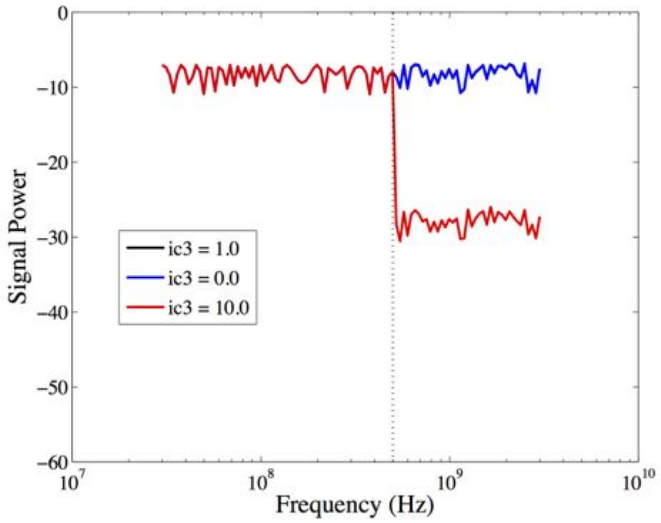

Figure 38. Output signal power vs. frequency for a input signal of amplitude 0.25 using a Heaviside function with cut-off frequency $f_c = 500$ MHz for three different cases when $f > f_c$: control, $i_{c3} = 0.0$, and $i_{c3} = 10.0$.

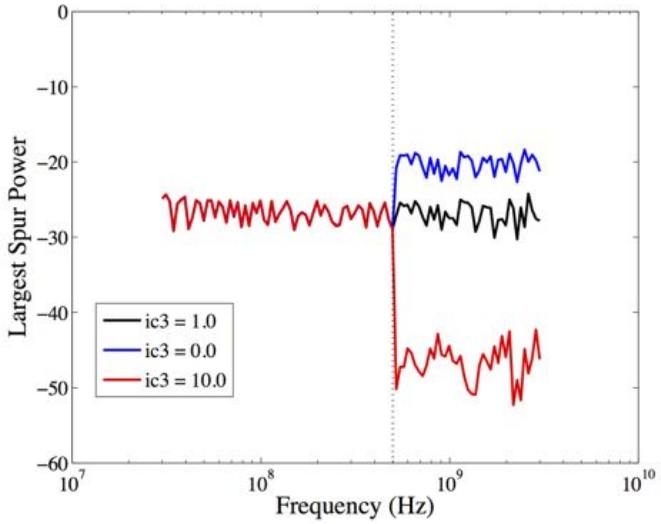

Figure 39. Magnitudes of the largest spurs vs. frequency for a input signal of amplitude 0.25 using a Heaviside function with cut-off frequency $f_c = 500$ MHz for three different cases when $f > f_c$: control, $i_{c3} = 0.0$, and $i_{c3} = 10.0$.

From these plots, we can determine that a frequency dependence can be modeled and visualized for a single bi-SQUID. The next step is to increase number of bi-SQUIDs from a single one to an array.

7. FREQUENCY DEPENDENCE OF A SERIES BI-SQUID ARRAY

In this section, we expand the frequency dependence to a series array of 25 bi-SQUIDs, and this time include a variance in the time scale parameter ω_0, which is dependent on the resistance (or inversely the conductance).

7.1 SERIES ARRAY MODEL

The system of equations without the temperature and capacitance terms is

$$\begin{aligned}
&(L_{1,k}+L_{2a,k})\frac{d\varphi_{1,k}}{d\tau}-L_{2b,k}\frac{d\varphi_{2,k}}{d\tau}-L_{1,k}\frac{d\varphi_{3,k}}{d\tau}\\
&\quad=L_{1b,k}i_B+\varphi_{e,k}+\varphi_{2,k}-\varphi_{1,k}-(L_{1,k}+L_{2a,k})i_{c1,k}\sin\varphi_{1,k}+L_{1,k}i_{c3,k}\sin\varphi_{3,k}\\
&\qquad+L_{2b,k}i_{c2,k}\sin\varphi_{2,k}+\sum_{i\neq k}\frac{M}{d_i^3a_i}(\varphi_{1,i}-\varphi_{2,i}-2\pi x_e a_i)\\
&L_2a\frac{d\varphi_{1,k}}{d\tau}-(L_{1,k}+L_{2b,k})\frac{d\varphi_{2,k}}{d\tau}-L_{1,k}\frac{d\varphi_{3,k}}{d\tau}\\
&\quad=-L_{1a,k}i_B+\varphi_{e,k}+\varphi_{2,k}-\varphi_{1,k}+(L_{1,k}+L_{2b,k})i_{c2,k}\sin\varphi_{2,k}+L_{1,k}i_{c3,k}\sin\varphi_{3,k}\\
&\qquad-L_{2a,k}i_{c1,k}\sin\varphi_{1,k}+\sum_{i\neq k}\frac{M}{d_i^3a_i}(\varphi_{1,i}-\varphi_{2,i}-2\pi x_e a_i)\\
&L_{2a,k}\frac{d\varphi_{1,k}}{d\tau}-L_{2b,k}\frac{d\varphi_{2,k}}{d\tau}+L_{3,k}\frac{d\varphi_{3,k}}{d\tau}\\
&\quad=\varphi_{2,k}-\varphi_{1,k}-\varphi_{3,k}-L_{2a,k}i_{c1,k}\sin\varphi_{1,k}+L_{2b,k}i_{c2,k}\sin\varphi_{2,k}-L_{3,k}i_{c3,k}\sin\varphi_{3,k},
\end{aligned}$$

where $\varphi_{1,k}$, $\varphi_{2,k}$ and $\varphi_{3,k}$ are the phases across the Josephson junction in each of the bi-SQUIDs, $k = 1, ..., N$ and $L_{1,k} = L_{1a,k} + L_{1b,k}$, $L_{3,k} = L_{3a,k} + L_{3b,k}$.

7.2 SIMULATION RESULTS

First, we varied the frequency and held i_{c3} and ω_0 constant with only nearest neighbor coupling for $M = 0.001$ (see Figure 40). Here, $x_e(f)$ is the top left plot, $\omega_0(f)$ is the top right, $P(f)$ is the bottom left, and $\Delta P(f)$ is the bottom right. The simulations were performed with $x_e = 0.25$, $N = 25$, and $M = 0.001$. The loops have a Gaussian distribution between $a = 0.52$ and $a = 1.52$ and the frequency is in megahertz. This shows some differences at each frequency, even if all other parameters are the same and may make it hard to determine the effects of each element.

To see if there was any distinct structures that would arise, we first varied i_{c3} and ω_0 together (see Figure 41). We used a ramp-type function instead of the Heaviside function from the last section. There is an overall increase in power of the signal, and an overall decrease in the power of the largest spurious signal. The different frequencies still vary quite a bit, however. To separate the variations caused by frequency, we held the frequency constant at 300 MHz in the next three simulations.

For the first of the three simulations with the frequency constant at 300 Mhz, we varied normalized parameter ω_0 from 0.5 to 1000 and held i_{c3} constant (see Figure 42). There is a peak around $\omega_0 \approx 1.0$, then a decrease until $\omega_0 \approx 20$ and a lower peak at $\omega_0 = 100$. The largest difference in power between the signal and the largest spur is at $\omega_0 \approx 1.0$.

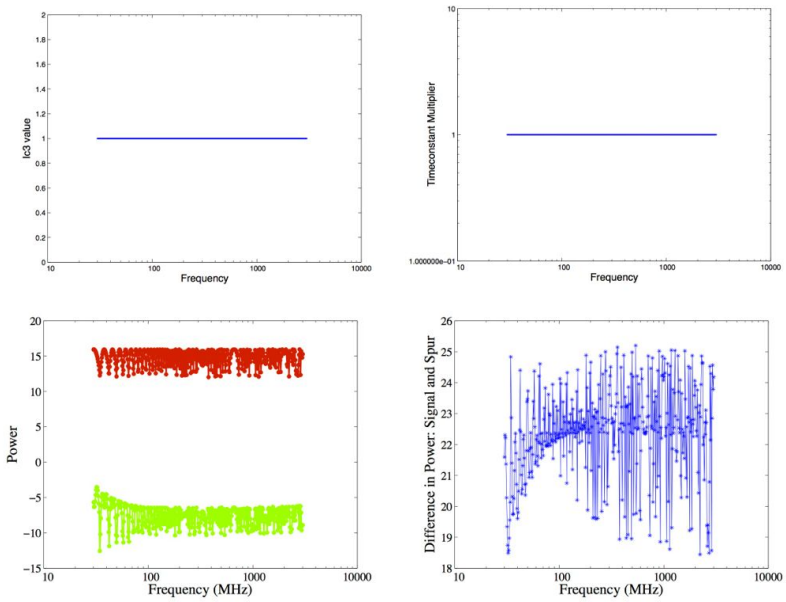

Figure 40. $i_{c3}(f)$ (top left), $\omega_0(f)$ (top right), $P(f)$ (bottom left), and $\Delta P(f)$ (bottom right) with $x_e = 0.25$, $N = 25$, $M = 0.001$, and a Gaussian distribution between $a = 0.52$ and $a = 1.52$.

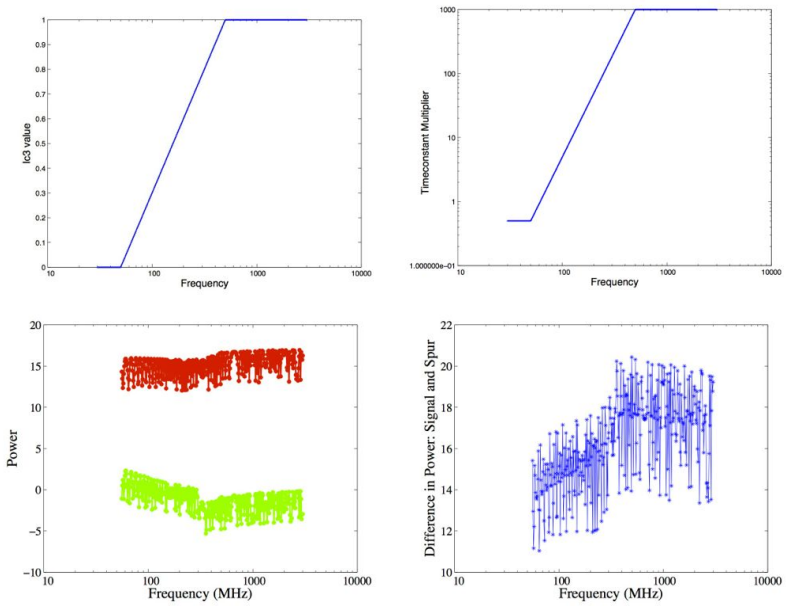

Figure 41. $i_{c3}(f)$ (top left), $\omega_0(f)$ (top right), $P(f)$ (bottom left), and $\Delta P(f)$ (bottom right) with $x_e = 0.25$, $N = 25$, $M = 0.001$, and a Gaussian distribution between $a = 0.52$ and $a = 1.52$.

For the second of three with the frequency constant at 300 Mhz, we varied i_{c3} from 0 to 1.0 and held ω_0 constant (see Figure 43). The signal power increases and largest spur power decreases continuously from $i_{c3} = [0, 1.0]$, resulting in the largest difference at $i_{c3} = 1.0$. Since this is the the value of i_{c3} for which the bi-SQUIDs have the greatest linearity, this was expected.

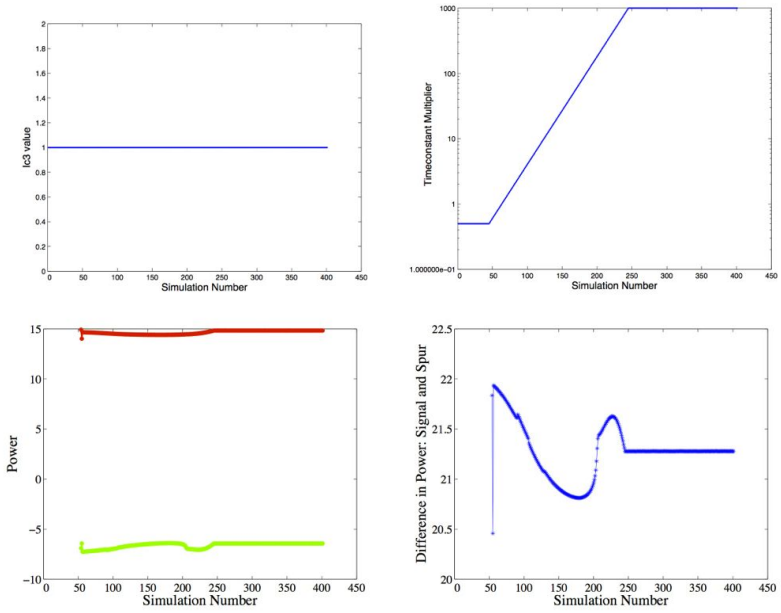

Figure 42. $i_{c3}(f)$ (top left), $\omega_0(f)$ (top right), $P(f)$ (bottom left), and $\Delta P(f)$ (bottom right) with $x_e = 0.25$, $N = 25$, $M = 0.001$, and a Gaussian distribution between $a = 0.52$ and $a = 1.52$.

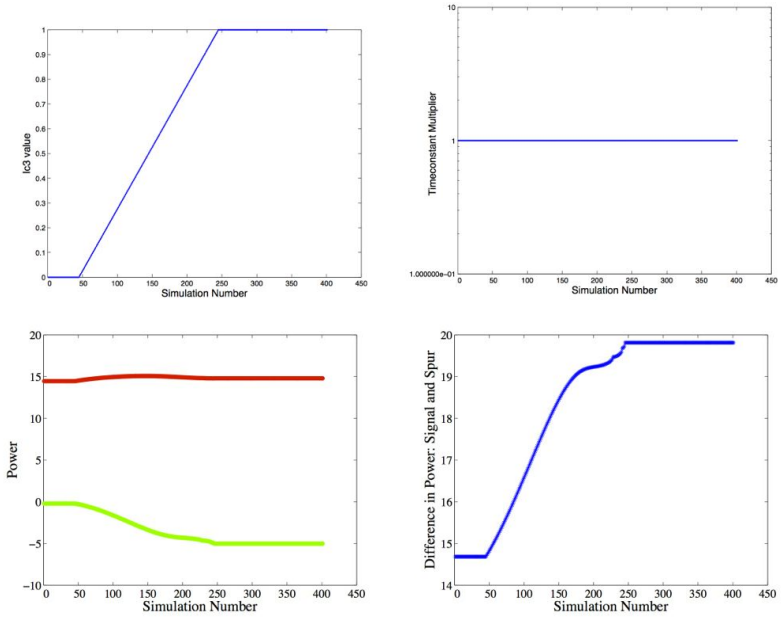

Figure 43. $i_{c3}(f)$ (top left), $\omega_0(f)$ (top right), $P(f)$ (bottom left), and $\Delta P(f)$ (bottom right) with $x_e = 0.25$, $N = 25$, $M = 0.001$, and a Gaussian distribution between $a = 0.52$ and $a = 1.52$.

Finally, we held the frequency constant at 300 Mhz and varied both i_{c3} and ω_0 together from 0 to 1.0 and from 0.5 to 1000, respectively (see Figure 44). The i_{c3} variations dominated the outcome, though the notch in the largest spur between simulations 200 and 250 from the ω_0 variance was visible. From this we can conclude that the value of the third-junction critical current has the largest effect on the signal detection, and this is what should be focused on, control through the frequency-dependent methods.

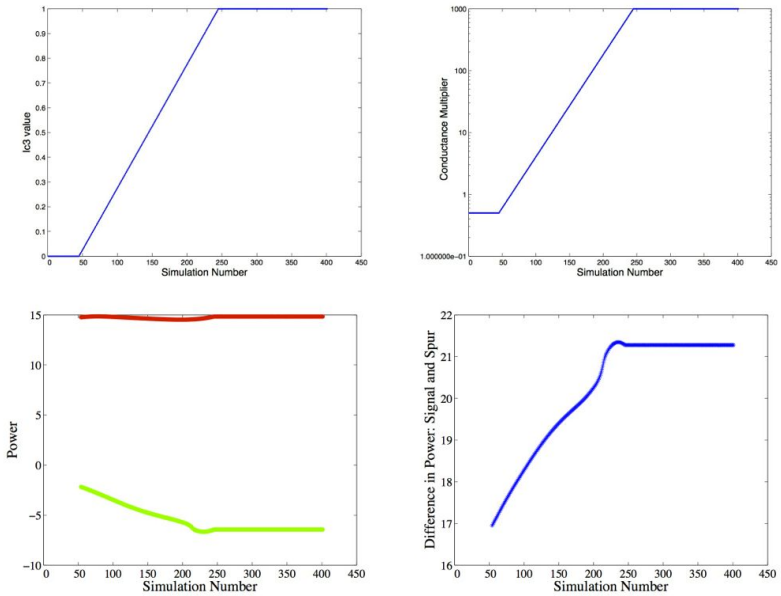

Figure 44. $i_{c3}(f)$ (top left), $\omega_0(f)$ (top right), $P(f)$ (bottom left), and $\Delta P(f)$ (bottom right) with $x_e = 0.25$, $N = 25$, $M = 0.001$, and a Gaussian distribution between $a = 0.52$ and $a = 1.52$.

The next step would be model the input of two signals at once and to increase the complexity to include the capacitance and temperature terms.

8. EXPERIMENTAL VALUES

To relate the model to realistic values that can be experimentally verified, some calculations need to be performed.

8.1 TIME CONSTANT

The first parameter calculated is the time constant that normalizes the theory. From the normalization of the phase equations that model a single bi-SQUID, it is determined that

$$\tau = \omega_0 t = \frac{2eI_0R_N}{\hbar}t.$$

Values for each of the parameters can be gathered or calculated:

$$\begin{aligned} I_c &\approx 0.25\text{mA} = 0.00025\text{A (example value)} \\ R_N &\approx 2.4\Omega \text{ (example value)} \\ \Phi_0 &= \frac{h}{2e} = 2.067834 \times 10^{-15}\text{Wb} \\ h &= 6.6260696 \times 10^{-34}\text{Js} \\ \hbar &= \frac{h}{2\pi} = 1.0545717 \times 10^{-34}\text{Js} \\ e &= 1.6021766 \times 10^{-19}\text{C} \\ V_c &= I_cR_N = 600\mu\text{V} = .0006\text{V}. \end{aligned}$$

Using the relations and values above, an approximate value for the time constant can be determined:

$$\omega_0 = \frac{2eI_0R_N}{\hbar} = \frac{2\pi V_c}{\Phi_0} = \frac{2\pi.0006\text{V}}{2.067834 \times 10^{-15}\text{Wb}} = 1.8231208 \times 10^{12}1/\text{s} \approx 10^{12}1/\text{s}.$$

Since approximate values are used for I_c and R_N, we can estimate that $\omega_0 \approx 10^{12}1/\text{s}$. This means that 1 unit of τ is equivalent to 10^{-12}s or a picosecond. In the code, values of τ are used from 0 to $2^{18}d\tau = 1048.576$, since $d\tau = 0.004$. Using the time constant determined in Equation (7), the time span translates to approximately 0 to 1.05 ns.

8.2 OUTPUT VOLTAGE IN VOLTS

From the relations in Equation (7), the response of the bi-SQUID in volts at a value of x_e can be determined as

$$V(t) = I_0R_N\frac{\dot{\varphi}_1 + \dot{\varphi}_2}{2} = 0.0003\,(\dot{\varphi}_1 + \dot{\varphi}_2)\,\text{Volts},$$

since

$$\omega_0\dot{\varphi}_i = \frac{2e}{\hbar}V_i.$$

8.3 AMPLITUDE OF INPUT SIGNAL

When running simulations, the minimum detectable signal has a normalized amplitude of $A = 0.000002$, and the largest signal detected without distortion has $A = 0.25$. The amplitude is in x_e, which is normalized by Φ_0. Thus, we can calculate the flux of the smallest signal detected as 4.135668×10^{-21}Wb and the flux of the largest signal without distortions as 5.169585×10^{-16}Wb.

To convert this value to volts, we determine the conversion from a $V(x_e)$ plot of a single bi-SQUID, which has no gain. For $I_c = 0.00025$A, $R_N = 2.4\Omega$ and the $V(x_e)$ shown in Figure 36, the maximum voltage is $V_{\text{max}} = 0.0006 * 0.9\text{V} = 0.00054$ volts. The $V(x_e)$ goes from 0 to 0.00054V in $0.5\phi_0$. From this we can determine the slope of the $V(x_e)$ as 5.223×10^{11}V/Wb. To get the signal strengths in volts, we multiply their flux by the slope of the single bi-SQUID AVR

$$S_{\text{min}} = 4.135668 \times 10^{-21}\text{Wb} * 5.223 \times 10^{11}\text{V/Wb} = 2.15 \times 10^{-9}\text{V} = 0.00215\mu\text{V}$$
$$S_{\text{max}} = 5.169585 \times 10^{-16}\text{Wb} * 5.223 \times 10^{11}\text{V/Wb} = 0.000269\text{V} = 269\mu\text{V}.$$

9. CONCLUSION

In this technical report, we reviewed the effects of capacitance and noise terms for a single junction and a single SQUID. Then we modeled a single bi-SQUID that has noise temperature and capacitance terms on the bisecting junction only. Next, we expanded to an array of 50 bi-SQUIDs. Finally, we look at effects of a frequency dependence of the third junction for a single bi-SQUID and an array of bi-SQUIDs. This study was done in order to understand the dynamics of HTS YBCO bi-SQUIDs and to investigate carefully designing the junctions to control the linearity and voltage swing of the anti-peak. The linearity and voltage swing are important for increased gain and improved accuracy, and frequency dependence could be used to implement filter-like capabilities.

From Section 2, we determined that for a single junction, capacitance is detrimental as is causes hysteresis. Some is tolerable if there is also a decrease in the junction resistance, since this counteracts the hysteresis arising from the capacitance. A large resistance negatively impacts junction performance and has an even stronger impact on hysteresis since $\beta_c \propto R^2$ while $\beta_c \propto C$. A small amount of temperature noise also decreases any hysteresis present; however, it also decreases the junction critical current (Figure 8). Overall, with this modeling, for the single junction dynamics, a decreased resistance (or alternatively an increased conductance) is desired.

For a single SQUID, the same conclusions as for a single junction were reached in Section 3. Even a small amount of hysteresis in the I-V curve destroyed the voltage swing in the $V(x_e)$ curve, which is the response we are trying to manipulate for signal detection. Large voltage swing equates to large signal gain and linearity equates to a large spurious free dynamic range. When hysteresis is present in the I-V curve, the bias current can be decreased to increase the voltage swing; however, this results in hysteresis in the $V(x_e)$ curve (Figure 13).

When we just include the capacitance and temperature terms on the bisecting Josephson junction, and leave the outer loop main junctions as ideal junctions, their impact on the $V(x_e)$ curve are decreased. This was explored in Section 4. The temperature term did counteract the effects of a large third-junction critical current on the $V(x_e)$ curve (becomes hysteretic) when there was small capacitance and resistance values (Figure 28). When the capacitance and resistance were increased, this was lessened. The effects of just modifying the third junction in the bi-SQUID are those that could arise from junctions either fabricated using a different method, such as ion beam milling or ion damage, or with junctions specifically designed to exploit certain properties, as with multiferroic junctions.

In Section 5, we explored series coupled arrays of bi-SQUIDs with the capacitance and temperature terms on the bisecting Josephson junction, and leaving the outer loop main junctions as ideal junctions. Gain is increased as we couple the SQUID or bi-SQUID devices together into arrays, so when we fabricate the prototype bi-SQUID sensor, we anticipate having tens of thousands of bi-SQUIDs in the array. As with the single bi-SQUID in Section 4, the impact of the capacitance and temperature terms on the $V(x_e)$ curve was decreased. From this we can surmise that if care is taken with the main two Josephson junctions, then the bisecting junction can be fabricated with an inferior method, and still result in a good device. An inferior method could be used to overcome design layout issues or for the properties gained by using them (i.e., multiferroics). The effects on the linearity of the anti-peak still need to be explored.

The frequency dependence of a single bi-SQUID was explored in Section 6. Here a frequency dependence was placed on the third-junction critical current in the form of a Heaviside function. We determined that we can control the signal detection if there is a frequency dependence on the critical current of the third junction. For a very basic example, if we could find a method that results in a large i_{c3} value (≈ 10) for large frequencies, and have a value close to $i_{c3} = 1.0$ in a range where the signal strength is small, and

$i_{c3} = 0$ elsewhere, we could have a device that acts like a low-pass filter and amplifies the signals further in the determined range.

For the array of bi-SQUIDs in Section 7, the value of the third-junction critical current had a much larger effect on the frequency dependence. These simulations were performed with different arrays in each simulation. To get a better comparison, the 25 loop sizes should be held constant throughout each different run.

This study, while extensive, is by no means exhaustive. Many configurations and parameter variations either were, explored but not presented here, or have not been attempted yet.

REFERENCES

1. P. Roediger, S. A. Cybart, and R. C. Dynes. 2013. "Fabrication of Arrays of Nano-superconducting Quantum Interference Devices using a Double-angle Processing Approach," *IEEE Transactions on Applied Superconductivity 23*:1100604.

2. V. K. Kornev, I. I. Soloviev, N. V. Klenov, and O. A. Mukhanov. 2009. "Bi-SQUID: A Novel Linearization Method for DC SQUID Voltage Response," *Superconductor Science and Technology 22*:114011.

3. A. B. Cawthorne, C. B. Whan, and C. J. Lobb. 1998. "Complex Dynamics of Resistively and Inductively Shunted Josephson Junctions," *Journal of Applied Physics 84*:1126.

4. R. Gross and A. Marx. 2005. "Chapter 3: Physics of Josephson Junctions: The Voltage State, Applied Superconductivity: Josephson Effect and Superconducting Electronics. Walther-Meiβner-Institut, Garching, Germany. Retrieved from www.wmi.badw.de/teaching/Lecturenotes/AS/AS_Chapter3.pdf

5. B. Ahlgren and D. Byström. 2011. "A Study of Josephson Junction Characteristics." Degree project in engineering physics. Department of Theoretical Physics Royal Institute of Technology (KTH), Stockholm, Sweden.

6. I. N. Askerzade. 2007. "Plasma Frequency of the Tunnel Josephson Junctions with Anharmonic Current-phase Relationship," *Technical Physics Letters 33*:723.

7. R. Gross and A. Marx. 2005. "Chapter 4: Superconducting Quantum Interference Devices, Applied Superconductivity: Josephson Effect and Superconducting Electronics," Walther-Meiβner-Institut, Garching, Germany. Retrieved from www.wmi.badw.de/teaching/Lecturenotes/AS/AS_Chapter4.pdf

8. C. H. Wu, Y. T. Chou, W. C. Kuo, J. H. Chen, L. M. Wang, J. C. Chen, K. L. Chen, U. C. Sou, H. C. Yang, and J. T. Jeng. 2008. "Fabrication and Characterization of High-T_c $YBa_2Cu_3O_{7-x}$ nanoSQUIDs Made by Focused Ion Beam Milling," *Nanotechnology 19*:315304.

9. C. H. Wu, F. J. Jhan, J. H. Chen, and J. T. Jeng. 2013. "High-T_c Josephson Junctions Fabricated by Focused Ion Beam Direct Milling," *Superconducting Science and Technology 26*:025010.

10. S. A. Cybart, T. N. Dalichaouch, S. M. Wu, S. M. Anton, J. A. Drisko, J. M. Parker, B. D. Harteneck, and R. C. Dynes. 2012. "Comparison of Measurements and Simulations of Series-parallel Incommensurate Area Superconducting Quantum Interference Device Arrays Fabricated from $YBa_2Cu_3O_{7-\delta}$ Ion Damage Josephson Junctions," *Journal of Applied Physics 112*:063911.

11. S. A. Cybart. 2005. "Planar Josephson Junctions and Arrays by Electron Beam Lithography and Ion Damage." Doctoral dissertation. University of Calfornia, San Diego. San Diego, CA.

12. C. Daumont. 2009. "Multiferroic Perovskites under Epitaxial Strain: The Case of $TbMnO_3$ Thin Films." Doctoral dissertation. Zernike Institute for Advanced Materials, University of Groningen, The Netherlands.

13. M. Gajek, M. Bibes, S. Fusil, K. Bouzehouane, J. Fontcuberta, A. Barthélémy, and A. Fert. 2007. "Tunnel Junctions with Multiferroic Barriers," *Nature Materials 6*:296–302.

14. S. Kawabata, Y. Asano, Y. Tanaka, A. A. Golubov, and S. Kashiwaya. 2010. "Josephson π State in a Ferromagnetic Insulator," *Physical Review Letters 104*:117002.

15. S. Liou, W. Kuo,1, Y. W. Suen, W. H. Hsieh, C. S. Wu, and C. D. Chen. 2007. “Shapiro Steps Observed in a Superconducting Single Electron Transistor,” *Chinese Journal of Physics 45*:230–236.

16. S. Berggren. 2012. “Computational and Mathematical Modeling of Coupled Superconducting Quantum Interference Devices.” Doctoral dissertation. San Diego State University, San Diego, CA, and Claremont Graduate University, Claremont, CA.

REPORT DOCUMENTATION PAGE

Form Approved
OMB No. 0704-01-0188

PLEASE DO NOT RETURN YOUR FORM TO THE ABOVE ADDRESS.

1. REPORT DATE *(DD-MM-YYYY)*	2. REPORT TYPE	3. DATES COVERED *(From - To)*
September 2014	Final	

4. TITLE AND SUBTITLE

Modeling the Effects of Varying the Capacitance, Resistance, Temperature, and Frequency Dependence for HTS Josephson Junctions, DC SQUIDs and DC bi-SQUIDS

5a. CONTRACT NUMBER

5b. GRANT NUMBER

5c. PROGRAM ELEMENT NUMBER

6. AUTHORS

Susan Berggren
Benjamin Taylor
Anna Leese De Escobar

5d. PROJECT NUMBER

5e. TASK NUMBER

5f. WORK UNIT NUMBER

7. PERFORMING ORGANIZATION NAME(S) AND ADDRESS(ES)

SSC Pacific, 53560 Hull Street, San Diego, CA 92152–5001

8. PERFORMING ORGANIZATION REPORT NUMBER

TR 2050

9. SPONSORING/MONITORING AGENCY NAME(S) AND ADDRESS(ES)

Naval Innovative Science and Engineering (NISE) Program (Applied Research)
SSC Pacific, 53560 Hull Street, San Diego, CA 92152–5001

10. SPONSOR/MONITOR'S ACRONYM(S)

11. SPONSOR/MONITOR'S REPORT NUMBER(S)

12. DISTRIBUTION/AVAILABILITY STATEMENT

Approved for public release.

13. SUPPLEMENTARY NOTES

14. ABSTRACT

The objective of this research was to explore the effects of altering the third junction in an array of bi-superconducting quantum interference devices (bi-SQUIDs) on the overall performance characteristics. The third junction could be altered by either fabricating it using a different method, such as ion beam milling or ion damage, or with junctions specifically designed to exploit certain properties, as with multiferroic junctions.

Based on the results of this study, we determined that a modification to the third junction is a viable approach to introduce a desired frequency dependence and/or control of the linearity and voltage swing of the anti-peak. This study, while extensive, was by no means exhaustive, and a significant amount of work remains to fully examine the different effects.

15. SUBJECT TERMS

Mission Area: Applied Research

superconductor modeling	frequency dependence	hysteresis
Bi-SQUID arrays	Josephson junctions	simulation

16. SECURITY CLASSIFICATION OF:			17. LIMITATION OF ABSTRACT	18. NUMBER OF PAGES	19a. NAME OF RESPONSIBLE PERSON
a. REPORT	b. ABSTRACT	c. THIS PAGE			Susan Berggren
U	U	U	U	50	19B. TELEPHONE NUMBER *(Include area code)* (619) 553-2063

INITIAL DISTRIBUTION

84300	Library	(2)
85300	Archive/Stock	(1)
71730	S. Berggren	(1)
71730	B. Taylor	(1)
71730	A. Leese De Escobar	(1)

Defense Technical Information Center
Fort Belvoir, VA 22060–6218 (1)

Approved for public release.

SSC Pacific
San Diego, CA 92152-5001